

A Study of 3CR Radio Galaxies from $z = 0.15$ to 0.65 . I. Evidence for an Evolutionary Relationship Between Quasars and Radio Galaxies

Michael Harvanek^{1,2}, E. Ellingson², & John T. Stocke²

*Center for Astrophysics and Space Astronomy, CB 389 University of Colorado, Boulder, Colorado, 80309-0389,
electronic mail: harvanek, stocke, e.elling@casa.colorado.edu*

and

George Rhee²

*Physics Department, University of Nevada, Las Vegas, NV, 89195
electronic mail: grhee@dawg.physics.unlv.edu*

ABSTRACT

Deep optical images have been gathered for a nearly complete sample of radio galaxies from the Revised 3rd Cambridge (3CR) Catalog in the redshift range $0.15 < z < 0.65$. Total and nuclear magnitudes and colors have been extracted. The richness of the galaxy clustering environment has also been quantified by calculating the amplitude of the galaxy-galaxy spatial covariance function (B_{gg}), showing overdensities ranging up to Abell class 0-1 clusters. These optical data are compared to similar data from an existing sample of radio-loud quasars in the same redshift range for the purpose of determining the relationship between radio galaxies and quasars. In the range $0.15 < z < 0.4$, we find that quasars and radio galaxies have significantly different environments in that only radio galaxies are found in rich cluster environments. This comparison appears to rule out the hypothesis that all quasars are radio galaxies viewed from a particular angle at the 97% confidence level (99.6% confidence level if N -galaxies are considered quasars). The existence of quasars in clusters at $z > 0.4$ supports the hypothesis that some radio-loud quasars may dim with time and evolve into radio galaxies with an e-folding time of ~ 0.9 Gyr. A compatible scenario is presented for this evolution in which the quasar dims due to the absence of low velocity interactions between the quasar host and companion galaxies which trigger quasar activity and/or a diminishing fuel supply caused by the more effective gas “sweeping” of a growing intracluster medium.

¹Current Address: Apache Point Observatory, 2001 Apache Point Rd., PO Box 59, Sunspot, NM, 88349-0059,
email: harvanek@apo.nmsu.edu

²Visiting Astronomer, Kitt Peak National Observatory, National Optical Astronomy Observatories, which is operated by the Association of Universities for Research in Astronomy, Inc. (AURA) under cooperative agreement with the National Science Foundation.

Subject headings: galaxies: active — galaxies: clusters: general — galaxies: evolution — galaxies: nuclei — galaxies: photometry — quasars: general

1. Introduction

Radio galaxies are one of the many types of active galactic nuclei (AGN) recognized today. Currently, the list of AGN types includes quasars, QSOs, radio galaxies (broad and narrow lined), Seyfert galaxies (types I and II) and blazars. The observational properties of the different types of AGN vary considerably, and although all are thought to be driven by a supermassive ($> 10^6$ solar mass) black hole at the nucleus of their host galaxy, the relationships among the various types of AGN are not well understood. The currently accepted model for radio-loud AGN invokes a supermassive black hole that powers a relativistic jet, creating Doppler-boosted, beamed radiation. Differences in the amount of obscuration of the AGN, orientation of the jet with respect to the line of sight, motion of the jet, properties of the black hole and evolution have all been used in various combinations to explain the differences in the properties of the various AGN types. However, to date, no one model has been able to explain them all. In fact, the “unification” of this diverse group of objects is currently one of the primary goals of extragalactic astronomy.

In an effort to further explore the unification of AGN, this work will examine one of the more controversial AGN relationships: that between quasars and radio galaxies. The radio sources associated with quasars are generally quite similar in both luminosity and morphology to the radio sources associated with the more powerful radio galaxies; typically, both are Fanaroff-Riley Type 2, or FR2, sources (Fanaroff & Riley 1974). Some differences in the radio properties do exist however. Radio galaxies have, on average, weaker radio cores (Miley 1980, Owen 1986), exhibit weaker radio jets (Owen 1986), and can have larger linear dimensions (Miley 1980) than quasars. The spectra of quasars are characterized by broad emission lines. The spectra of a few radio galaxies show broad emission lines while most show only narrow emission lines.” Quasars are luminous in X-rays (e.g., Zamorani et al. 1981; Worrall 1987) whereas radio galaxy AGN are comparatively dim (e.g., Feigelson & Berg 1983). While many are found in elliptical host galaxies, a significant number of quasars (Smith et al. 1986; Hutchings 1987; Stockton & MacKenty 1987) and powerful radio galaxies (Heckman et al. 1986; Hutchings 1987; de Koff et al. 1996) are found in hosts with peculiar optical morphologies, indicating interacting and/or merging systems. Finally, more luminous quasars and radio galaxies (e.g., those from the 3CR catalogs of Laing et al. (1983) and Spinrad et al. (1991)) have remarkably similar redshift distributions at $z \gtrsim 0.4$ (Longair 1985; Barthel 1989). All these various relationships between quasars and radio galaxies, along with their differing projected physical sizes and optical polarization properties (see Barthel (1989) and references therein) and evidence for the preferred orientation of some quasars led Barthel (1989) to propose that quasars and FR2 type radio galaxies are the same type of object viewed from a different orientation angle. Since their properties suggest that quasars are beamed toward us, this hypothesis proposes that quasars are FR2 type radio galaxies with their jets oriented closer to our

line of sight (within $\sim 45^\circ$).

However, the work of Yee & Green (1987, hereafter YG), Ellingson, Yee & Green (1991a, hereafter EYG) and Yee & Ellingson (1993, hereafter YE93) suggests another possibility. These studies indicate that while up to one third of optically bright, radio-loud quasars at $z \sim 0.6$ are found in Abell class 0 or richer clusters, a much smaller fraction of lower redshift quasars are found in rich environments. In addition, they found that the brightest quasars which inhabit clusters at $z \sim 0.4$ are several magnitudes fainter than quasars in clusters at higher redshifts. The only radio-powerful AGN found in clusters at low redshifts are radio galaxies. In contrast, the fraction and luminosity of the brightest quasars in poorer environments change relatively little over these epochs. This suggests that environment strongly affects quasar evolution, and that quasars are rapidly disappearing from rich clusters over this redshift range. Based on their findings, EYG proposed that quasars may dim with time and eventually fade to become radio galaxies. This will be referred to as the evolutionary hypothesis of EYG. Note that this hypothesis is not wholly inconsistent with the beaming phenomenon—only with viewing angle being the *sole* explanation for the different AGN classes. In the evolutionary hypothesis, the nuclear properties of some individual objects may be affected by beaming, but there is also a fundamental evolutionary connection between luminous quasars and radio galaxies.

One key to testing these competing hypotheses is the galaxy environments of the FR2 radio galaxies. Assuming that the richness of the galaxy environment is independent of the orientation angle to the line of sight (i.e., the cluster richness remains the same regardless of the angle from which it is viewed), if quasars and FR2 radio galaxies are the same type of object viewed from a different angle, the galaxy environments of quasars and FR2 radio galaxies at the same redshift should be similar. EYG found essentially no optically bright quasars in clusters at $0.15 < z < 0.4$; thus, the orientation angle hypothesis of Barthel (1989) predicts that no FR2 radio galaxies in this redshift range should be found in clusters. However, if quasars evolve into radio galaxies, the galaxy environments of radio galaxies at $0.15 < z < 0.4$ should be similar to that of quasars at some earlier epoch. Since EYG found quasars in both rich and poor environments at $z > 0.4$, their evolutionary hypothesis predicts that the percentage of FR2 radio galaxies found in rich environments at $0.15 < z < 0.4$ should be similar to the percentage of quasars found in rich environments at some epoch $z > 0.4$.

However, consistent data on the galaxy environments of FR2 radio galaxies at $0.15 < z < 0.4$ has been lacking. Although a number of studies of the environments of radio galaxies have been conducted previously (Lilly & Prestage 1987; Prestage & Peacock 1988; Yates, Miller & Peacock 1989; hereafter YMP, Hill & Lilly 1991; hereafter HL; Allington-Smith et al. 1993; Zirbel 1997), much of the data collected were for radio galaxies at higher or lower redshifts. (Note that data for radio galaxies at $z < 0.15$ are abundant. However, since quasars are not found at $z < 0.15$, this data cannot be used to test Barthel's hypothesis.) The studies that did provide adequate coverage over the relevant redshift range (Allington-Smith et al. 1993; Zirbel 1997) used different filters and quantified the richness of the galaxy environment in a somewhat different manner.

Thus, we obtained deep optical images of a sample of 39 radio-powerful 3CR AGN in this redshift range to determine the properties of the AGN nuclear sources and their environments. In Section 2 the radio galaxy and quasar samples are presented. The observations, reductions, photometry and other data processing are discussed in Section 3. In Section 4 the B_{gg} parameter, which quantifies the richness of the clustering environment, is presented in some detail. Incorporation of other clustering data is discussed and the environmental data is tabulated. In Section 5 the properties of the radio galaxies are compared to the properties of quasars and the results of this comparison are used to determine whether the orientation angle hypothesis of Barthel (1989) or the evolutionary hypothesis of EYG can better explain the relationship between quasar and radio galaxy environments. A summary of the results is given in Section 6 and a scenario which accounts for them is proposed. Values of $H_0 = 50 \text{ km s}^{-1} \text{ Mpc}^{-1}$ and $q_0 = 0$ (or 0.02) are assumed throughout this work for consistency with EYG. In a companion paper (Harvanek & Stocke 2001, Paper 2 hereafter) we study the extended radio structure of the sources in this sample.

2. The Samples

2.1. The Observed Sample

The sample chosen for this study was drawn from the 3CR radio galaxies and quasars with $0.15 < z < 0.65$ and $|b| \geq 15^\circ$ that are listed in the Revised 3C Catalog of Radio Sources of Smith, Spinrad & Smith (1976) as updated by Spinrad et al. (1985) and Spinrad et al. (1991). This catalog was chosen as the source of our sample for several reasons. Having originated from the 3CR radio catalog (a list of more than 300 of the brightest radio sources observed at 178 MHz by Bennett (1962)), this catalog ensures that any source at $z > 0.15$ chosen from it will be comparable in radio power to the sources in the quasar comparison sample of YE93 (see below). Furthermore, since the catalog is nearly complete (for sources having 178 MHz flux ≥ 10.9 Jy on the scale of Baars et al. (1977)) and almost entirely identified ($> 91\%$; Spinrad et al. (1991), and objects with $|b| \geq 15^\circ$ are essentially 100% complete) it provides a very comprehensive listing of such sources. Choosing sources from only one flux-limited catalog also helps ensure a uniform sample. The galactic latitude was restricted because the large number of stars and the possibility of uneven extinction near the galactic plane make the measurement of the galaxy environment more uncertain.

Table 1 shows the sample taken from the 3CR catalog and tabulates some of the more useful properties. There are 66 radio galaxies and 14 quasars listed. However, one of the galaxies, 3C 258, was discovered to contain what is believed to be a distant background quasar in its spectrum (A. Dey, private communication). Since the angular size of 3C 258 is quite small for a source at a redshift of $z = 0.165$, it is likely that the radio source is associated with the background object. Thus, this object has been removed from the sample and is excluded from any of the analysis presented in this study.

Listed in Table 1 along with the sources are their optical positions, redshifts, 178 MHz flux

densities on the scale of Baars et al. (1977), and spectral indices between 178 and 750 MHz. (The spectral index α is defined here in the sense $S \propto \nu^{-\alpha}$.) The optical positions and redshifts were taken from Spinrad et al. (1991) except for the optical positions of 3C 225B and 3C 435A, which were taken from Giovannini et al. (1988) (from the cross on the radio map) and McCarthy, van Breugel, & Spinrad (1989), respectively. The 178 MHz flux densities were taken from Laing et al. (1983) if available. If not available in Laing et al. (1983), the values given in Kellermann et al. (1969) were used for most other sources. The 178 MHz flux densities for 3C 99, 3C 258, and 3C 306.1 were taken from Gower et al. (1967) and that for 3C 268.2 was taken from Pilkington & Scott (1965) (all available from the NASA/IPAC Extragalactic Database, 1997) because their values in Kellermann et al. (1969) are likely contaminated by nearby sources. The guidelines for choosing the most appropriate 178 MHz flux density for any given source are discussed in detail in Laing et al. (1983). All fluxes were adjusted to the scale of Baars et al. (1977) using the corrections given in Laing & Peacock (1980). Spectral indices were computed using the 178 MHz flux densities given here and 750 MHz flux densities from Kellermann et al. (1969). Comparison of our spectral index values to those of Laing et al. (1983) shows perfect agreement for all 48 objects common to both samples. For one source, 3C 435A, the 178 MHz flux density and the spectral index were not directly available because the separation of 3C 435 into the two unrelated sources, 3C 435A and 3C 435B, occurred after the work of Kellermann et al. (1969) and we were unable to find these values in more current literature. Since no other data were available, the spectral index of 3C 435A listed in Table 1 is that of the combined source, 3C 435. The 178 MHz flux density was computed using the 1500 MHz flux density of 3C 435A from McCarthy, van Breugel, & Spinrad (1989) and a spectral index for the combined source calculated from fluxes at the appropriate frequencies taken from Kellermann et al. (1969).

Also included in Table 1 are the rest frame luminosity (i.e., power) at 178 MHz, the log of this rest frame luminosity, the optical spectral type of the source (i.e., the “optical class”) and the object type of the source. The rest frame luminosity was calculated from the 178 MHz flux density, the spectral index and the redshift, assuming a Friedmann cosmology with $H_0 = 50 \text{ km s}^{-1} \text{ Mpc}^{-1}$ and $q_0 = 0$. All sources in this sample have a rest frame luminosity above (most well above) the nominal boundary between FR1 and FR2 type radio sources (Fanaroff & Riley 1974). The radio morphology of these sources mostly confirms this FR2 luminosity classification (see also Paper 2 for a more detailed analysis and discussion). The same is true of the quasar comparison sample of YE93 discussed below. We classify each object as “broad-line” (B), “narrow-line” (N) or “low-excitation” (E). Except for 3C 234 and 3C 381, the optical type was taken directly from Jackson & Rawlings (1997) who use a slightly different notation than that used here. Their “quasar/weak quasar” (Q/WQ) classification is equivalent to our broad-line (B) type. Similarly, their “high-excitation galaxy” (HEG) corresponds to our narrow line (N) type and their “low-excitation galaxy” (LEG) is the low-excitation (E) type. The references for the optical spectra on which these classifications are based can be found in Jackson & Rawlings (1997). The optical type for 3C 234 and 3C 381 was taken from Hardcastle et al. (1997) who also provide the references for the optical spectra from which these classifications are determined. The object types are galaxy (GAL), N-galaxy (N) and

quasar (QSO) and were taken directly from Spinrad et al. (1991).

2.2. The Quasar Comparison Sample

For the comparison study, we have utilized the quasar sample of YE93 which contains 65 quasars with $z < 0.65$ and $|b_{II}| \geq 30^\circ$, of which 10 are 3CR sources and most of the remainder are from the 4C and Parkes catalogs. Values of redshift, absolute nuclear B magnitude and B_{gq} (quasar-galaxy two point correlation function amplitudes; see Section 4) are provided by YE93 and for the comparison study we adopt their values directly. When combined with the 3CR sample discussed above, there are a total of 69 quasars and 65 radio galaxies in this study.

3. Observations and Reductions

All optical imaging data were obtained at the 0.9 m and 2.1 m telescopes of the National Optical Astronomy Observatories (NOAO) at the Kitt Peak National Observatory (KPNO). The lower z subsample ($0.15 < z < 0.35$) was observed with the smaller telescope (FOV $\sim 23'$ on a side) while the higher z subsample ($0.35 < z < 0.65$) was observed with the larger telescope (FOV $\sim 5'$ on a side).

The optical observations are listed in Table 2. The Gunn r and Gunn g filters were used for the observations because they match those of the background galaxy counts (Yee et al. 1986, as updated by H. Yee, private communication) and allow for a direct comparison with the quasar work. The integration times are typically 1800 sec in r and 3600 sec in g to yield a completeness magnitude 2-3 mags dimmer than M^* ($M_r^* \sim -22.0$; the combination of k-correction plus moderate luminosity evolution keeps this value approximately constant over the redshift range of interest.) The 5σ limiting magnitude for each field is listed in Table 2. The completeness magnitude is estimated to be ~ 0.8 mag brighter than the 5σ limiting magnitude (Yee, Ellingson & Carlberg 1996).

The identification and classification of all objects in each field and the calculation of an instrumental magnitude for each object were performed using the Picture Processing Package (PPP) software developed by Yee (1991), and further described in Yee, Ellingson & Carlberg (1996). To calibrate the photometry, standard stars from Kent (1985) were observed at several different times during each night of each of the observing runs. Observational uncertainties are typically 0.03-0.1 mag. The observed total apparent magnitudes were corrected for Galactic reddening by using (A_λ/A_V) given by Cardelli, Clayton & Mathis (1989) with the currently accepted value of $R_V = 3.1 \pm 0.1$ and values of $E(B-V)$ for each field taken from Burstein & Heiles (1982). Gunn r absolute magnitudes were k-corrected using the values given in Sebok (1986) for E/S0 type galaxies as a function of z and Gunn g magnitudes were corrected using the tables from Fukugita et al. (1995). Total magnitudes (apparent and absolute) and observed $g-r$ colors for the radio

galaxies are given in Table 3. Those for the quasars are found in Table 4.

Total magnitudes marked with a colon were not obtained from our data. They are estimates based on the brighter of m and m_{15} (total magnitude and magnitude inside 15 kpc, respectively) given in de Koff et al. (1996). These magnitudes were obtained with the Hubble Space Telescope (HST) using the broad-band F702W filter and were converted to Gunn r using the conversions given in Fukugita et al. (1995) for E type galaxies as a function of z . Due to low exposure times and the combination of the extremely high resolution and small pixel size of HST, the magnitudes taken from de Koff et al. (1996) may be dimmer than the actual total magnitudes and so entries marked with a colon in Table 3 should be used with caution.

To estimate the nuclear magnitudes for the radio galaxies, we used m_1 (the magnitude within a 1 kpc radius for $H_0 = 75 \text{ km s}^{-1} \text{ Mpc}^{-1}$, $q_0 = 0.5$, which corresponds to 0.2-0.36" for this redshift range) from de Koff et al. (1996), appropriately corrected to obtain M_B for $H_0 = 50 \text{ km s}^{-1} \text{ Mpc}^{-1}$, assuming a typical power-law AGN spectrum with $\alpha = -0.5$ (YE93), equivalent to a $g - r$ color of -0.11 mag. However, these m_1 magnitudes will contain a small contribution from the host galaxy, although the exact amount is unknown without a detailed knowledge of the inner surface brightness profile. If a deVaucouleurs profile (de Vaucouleurs 1948) is assumed, the galaxy contribution will be typically a few tenths of a mag at most. Therefore, we have used m_1 mags as an estimate of the nuclear magnitudes for all those galaxies in Table 1 whose optical class is N or B. For N or B class radio galaxies, ground-based spectra through apertures considerably larger than 1 kpc are dominated by non-thermal continuum. Additionally, a visual inspection of the spectra in Tadhunter et al. (1993) for those galaxies in Table 1 left unclassified by Jackson & Rawlings (1997) finds their ground-based spectra likewise non-thermally dominated. The spectra of galaxies classified as E type, in some cases (e.g., 3C 348), but not all show optical spectra dominated by host galaxy starlight (Tadhunter et al. 1993). To be conservative, we have listed m_1 mags as a limit on the nuclear brightness of galaxies of type E in Table 3. This relative inaccuracy in our nuclear magnitude estimates does not affect our final results.

4. Clustering Analysis

This work utilizes B_{gg} , the amplitude of the galaxy-galaxy spatial covariance function, as a quantification of the richness of the clustering environment around a given object. Given a cosmology, an assumed evolution of the galaxy luminosity function and measured mean background galaxy counts, this parameter reflects the galaxy overdensity around a given object, correcting for the expected spatial and luminosity distributions of field galaxies and of the associated cluster galaxies at the redshift of the object.

This parameter is described in detail in Longair & Seldner (1979) and the specific technique used in obtaining the actual values of B_{gg} is described in Yee & Green (1987) and EYG. Briefly, the technique is as follows. All galaxies within 0.5 Mpc of the radio source brighter than some

magnitude are counted. Then the expected number of background galaxies in that area down to the same magnitude is subtracted. The number of excess galaxies is normalized to an evolved galaxy luminosity function at the redshift of the object and then converted to B_{gg} assuming a form for the spatial distribution of galaxies.

As explained in EYG, the 0.5 Mpc counting radius is chosen to provide good contrast between cluster and foreground/background galaxies and to minimize the effects of the variation of the actual spatial distribution of the cluster galaxies from the assumed form. The magnitude limit for galaxy counting is determined for each field individually and is taken to be the brighter of the “completeness” magnitude, m_{comp} , or $M_r^* + 2.5$. Background galaxy counts are those of Yee et al. (1996,1998). The evolving galaxy luminosity function used to normalize the excess galaxies includes moderate galaxy evolution of $M_*(z) \sim z$ (EYG). Finally, the distribution of the excess galaxies is assumed to be the standard cluster galaxy power law ($r^{-\gamma}$ where $\gamma = 1.77$). This originates from the angular distribution of Seldner & Peebles (1978) and was used by both Yee & Green (1987) and EYG. Yee & Green (1987) show this assumption is consistent with their results.

It should be noted that although B_{gg} is a measure of the excess galaxies around a given object, a large value of B_{gg} does not prove absolutely that there is a cluster around any individual object. The excess galaxies could be due to an anomalous overdensity of foreground and/or background galaxies in that region of the sky. Although galaxy colors can be used as an indication of the redshift of the excess galaxies, only spectroscopic observations can completely confirm cluster membership. For those who are more familiar with the cluster richness classification of Abell (1958): B_{gg} values of 600 ± 200 , 1000 ± 200 , 1400 ± 200 , and 1800 ± 200 Mpc^{1.77} are comparable to Abell richness classes 0, 1, 2, and 3, respectively (Yee & López-Cruz 1999). EYG chose $B_{gg} = 500$ Mpc^{1.77} to define the boundary between rich and poor environments because, at the time, it was thought to be the division between Abell richness classes 0 and 1 (Prestage & Peacock 1988, 1989). We adopt this boundary for consistency with the earlier work and show below that this choice does not affect our results significantly.

The total uncertainty in B_{gg} is given by $\Delta B_{gg}/B_{gg} = (N_{net} + 1.3^2 N_b)^{1/2}/N_{net}$ (Yee & López-Cruz 1999) where N_b is the expected number of background galaxy counts and $N_{net} = N_{total} - N_b$ is the number of excess galaxy counts. This uncertainty is obtained by adding two terms in quadrature. The first term, $(N_{net})^{1/2}/N_{net}$, is the internal statistical error in sampling the associated cluster galaxy luminosity function using a finite number of galaxies. The second term, $1.3(N_b)^{1/2}/N_{net}$ (EYG), is the error due to the uncertainty in the background galaxy counts. The factor of 1.3 is an empirical value that accounts for the clustering of the background galaxies which causes the error in the background galaxy counts to deviate from a Poisson error. This factor is discussed in detail in Yee et al. (1986). The error in B_{gg} is often quite a substantial fraction of the B_{gg} value due to the small number of “excess” galaxies relative to the expected number of field galaxies. Two of the quasar fields we observed (3C 323.1 and 3C 351) were also observed by YE93. A comparison of our B_{gg} values with theirs shows differences within the uncertainties that are easily attributable to differences in the limiting magnitudes.

4.1. Incorporation of Other Clustering Data

We have measured B_{gg} for 39 of the 79 fields in our sample. However, measures of the excess galaxies surrounding many additional objects exist in the literature in one form or another and have been incorporated into this study. Table 5 provides a comparison between our method of measuring B_{gg} and the other methods of measuring the number of excess galaxies. The differences between methods and the conversions to our B_{gg} values are discussed below for each method listed in Table 5.

4.1.1. *Yee & Ellingson (1993)*

Nuclear magnitudes and B_{gg} values for 63 quasars (8 of which are 3CR sources) with $0.15 < z < 0.7$ were taken directly from YE93, which includes the samples used in EYG. These B_{gg} values were obtained in a manner almost identical to our own. Some of their values (those taken from YG and Yee & Green (1984)) were calculated using $q_0 = 0.5$ with a slightly different luminosity function (that of Sebok (1986) rather than the luminosity function of King & Ellis (1985) that we used; see YG) and with slightly different background counts, but these differences are minor. We have thus taken their values without any correction. As mentioned above, comparisons of B_{gg} values for objects in common agree to within the uncertainties.

4.1.2. *Zirbel (1997)*

Zirbel (1997) observed a sample of radio galaxies (of which 27 are in the 3CR sample in our redshift range) and quantified the galaxy environment using $N_{0.5}^{-19}$ (or “richness”): the number of excess galaxies brighter than $M_V = -19$ within a 0.5 Mpc radius of the object. The main differences between this method and our method are that the images are in V rather than Gunn r , the limiting magnitude is fixed for all fields, and galaxies that are -0.6 mag bluer or 0.2 mag redder than an elliptical galaxy of the same absolute magnitude are excluded from the excess galaxy counts. Since these galaxies are red, faint galaxies that would be detected in Gunn r may not be detected in V. The fixed limiting magnitude of $M_V = -19$ means that we tend to count galaxies down to fainter magnitudes, especially at lower redshifts ($z < 0.3$), but this should be accounted for in the normalization. The effect of excluding galaxies with anomalous colors is to reduce the number of excess galaxies. So, in general, we expect the number of excess galaxies measured by Zirbel (1997) to be less than ours. Since B_{gg} is directly proportional to the number of excess galaxies, we expect the $N_{0.5}^{-19}$ values of Zirbel (1997) to be converted to our B_{gg} values by a multiplicative constant. Since a correction for the luminosity evolution of the galaxies is made by Zirbel (1997) (see Allington-Smith et al. (1993) for details), this multiplicative constant is expected to be the same for all fields regardless of redshift. However, the differences between the two methods discussed above will cause a slight variation in this multiplicative constant from field to field and

so there will be some scatter around the actual conversion value.

In order to determine this conversion constant, a weighted least squares linear fit of Zirbel’s “richness” values to our B_{gg} values was performed using 13 objects for which we both had data. The fit was forced through the point (0,0) because zero excess galaxies should give $B_{gg} = 0$. The resulting conversion is $B_{gg} = 38N_{0.5}^{-19}$. The fit and the data points with their error bars are shown in Figure 1. The 1σ error bars for all but 3 of the points overlap the fit and the farthest of these 3 points (3C 348) lies within 2σ of the fit.

4.1.3. *Yates, Miller & Peacock (1989; YMP)*

This work includes data from 14 3CR radio galaxies in our redshift range. The B_{gg} values are the same quantity that we calculate. However, their values are not directly comparable to ours due to differences in methodology and so a conversion is still required. While their model 2b is the closest to our work ($q_0 = 0$, a King & Ellis (1985) luminosity function, YG normalization and evolution), they do not distinguish between stars and galaxies when counting objects, the area over which they count objects varies from field to field and their computation of the completeness magnitude is different from ours. Although the inclusion of stars to their number counts sounds like a crucial difference, it should be accounted for by their “local” (5' to 10' offset) measurement of background objects (stars and galaxies). This assumes that there are no large differences in the stellar number density between an object field and its offset frame. However, not directly eliminating the stars from the analysis increases the random uncertainty in B_{gg} . Yates, Miller & Peacock (1989) also take their completeness magnitude to be at the peak of their galaxy number distribution whereas we take it to be where the galaxy number distribution begins to drop below the expected linear form. This will cause Yates, Miller & Peacock (1989) to overestimate their completeness magnitude, giving them lower counts and a lower value of B_{gg} than ours for the same completeness magnitude. However, the non-uniform variation of both our completeness magnitude and that of Yates, Miller & Peacock (1989) from field to field prevents this from appearing as a systematic difference in the objects we both observed.

We can attempt to model the effects of the differences between our method and that of Yates, Miller & Peacock (1989) as an additive offset between the two B_{gg} values. Thus, we look for a conversion of the form: $\{\text{our } B_{gg}\} = \{\text{YMP } B_{gg}\} + \text{constant}$. Note, however, that the variation of the differences in the two methods from field to field may cause this offset to vary. An average offset of 70 was determined from 5 of the 7 objects for which we both had data. The remaining two objects (3C 346 and 3C 348; the uppermost points of Figure 2) were not used in the determination of this offset because they both had extremely small counting areas when compared to ours (smaller by a factor ~ 3) and so represented extreme rather than typical differences. A comparison of this “average offset” conversion to a weighted least squares linear fit to the same 5 points is shown in Figure 2. The offset conversion is given by the solid line. The two lines agree to within their error bars ($y = x + 70 \pm 147$ vs. $y = 0.91 \pm 0.54 \times x + 105 \pm 73$) and when the size of the error bars of the

points is considered, the difference between the two fits is quite small. Only 3C 348 is noticeably offset from the fit and it is still well within 2σ .

4.1.4. Hill & Lilly (1991; HL)

Hill & Lilly (1991) observed a sample of radio galaxies at $z \sim 0.5$, 13 of which are included in this study. Their measurement of $N_{0.5}$ is derived from the number of excess galaxies within a 0.5 Mpc radius of the object within the magnitude range m_1 to $m_1 + 3$ where m_1 is the magnitude of the object. We note that this method does include a built-in correction for galaxy evolution and k-corrections, as long as the radio galaxies can be considered typical of cluster galaxies. This quantity is computed using $q_0 = 0.5$. Another listed quantity, $N_{0.5}^M$, is the same as $N_{0.5}$ except that the mean m_R - z relation for the object is used as m_1 rather than the magnitude of the object itself. A third tabulated quantity, $N_{0.5}^0$, is the same as $N_{0.5}$ except that $q_0 = 0$ was used in the calculation. Although this third quantity is a closer match to our value of q_0 , the second quantity is more consistent with our method of determining the limiting magnitude. Using the $N_{0.5}^M$ values, the differences between our method and that of Hill & Lilly (1991) are the different value of q_0 , the slightly different optical waveband, variations in the limiting magnitude from field to field, and the fact that they do not distinguish between stars and galaxies. The effects of varying q_0 are negligible compared with the uncertainties. The difference in optical waveband is small (R vs. Gunn r), and should not systematically affect the results as long as both field and background counts are observed in the same band. Varying the limiting magnitude should have no systematic effect on the results, but can produce statistical variations in different measurements for individual objects, depending on how deep the luminosity function is sampled. Finally, as with Yates, Miller & Peacock (1989) above, the local measurement of background objects should account for stars not being removed but the potential for much larger errors is increased.

As with the $N_{0.5}^{-19}$ values of Zirbel (1997), we expect the conversion of the Hill & Lilly (1991) $N_{0.5}^M$ values to our B_{gg} to be in the form of a multiplicative constant. Hill & Lilly (1991) account for luminosity evolution by using the radio galaxy magnitude to define an epoch-invariant point on the luminosity function and then referencing the magnitudes of all galaxies in the counting region of the field to that of the radio galaxy. They note that this method yields values that are $\sim 20\%$ higher than those from the method that we have adopted. Thus, the conversion constant might actually be a function of redshift. However, the objects in Hill & Lilly (1991) that are in our sample have a relatively narrow redshift range ($z = 0.367$ to $z = 0.5524$) and so we assume a single multiplicative constant for the conversion of all values regardless of redshift. Although we had no data in common with Hill & Lilly (1991), we had 1 B_{gg} value from YE93 and 10 converted B_{gg} values from Zirbel (1997) that overlapped with the Hill & Lilly (1991) data. A weighted least squares linear fit forced through the point (0,0) was performed using all 11 of these objects, resulting in the conversion $B_{gg} = 33N_{0.5}^M$. The fit and the data points with their error bars are shown in Figure 3. This conversion lies between the empirical conversion ($B_{gg} = 30N_{0.5}$) and the theoretical conversion ($B_{gg} = 34N_{0.5}$)

given in Hill & Lilly (1991). Also, the somewhat lower conversion factor of the Hill & Lilly (1991) $N_{0.5}^M$ values as compared to that of the Zirbel (1997) $N_{0.5}^{-19}$ values (33 vs. 38) is consistent with the relationship between these values quoted in Allington-Smith et al. (1993), to within the error bars.

4.2. Summary of All Clustering Data

A compilation of the B_{gg} values from all the methods discussed above is given in Table 6. Discrepancies and uncertainties are discussed in the notes following the table and a key to the references is given after the notes. Errors for our values were discussed at the beginning of Section 4. Errors for the YE93 values were taken directly from the literature. Errors for the converted B_{gg} values (those from Zirbel (1997), Hill & Lilly (1991) and Yates, Miller & Peacock (1989)) were computed by converting the original 1σ values to B_{gg} values and using this spread in the converted B_{gg} value as the error.

“Adopted” B_{gg} values are listed in Table 7. Sixty five of the 79 objects in this complete 3CR sample have B_{gg} values. Because the absence of B_{gg} data is due entirely to the absence of photometric images and because the order in which objects were observed was random, there is no bias introduced due to this incompleteness in the B_{gg} data. In the absence of our own value, the value from YE93 was used in Table 7, if available; otherwise converted B_{gg} values were used. Since we had no data in common with Hill & Lilly (1991), this conversion is indirect and so the values of Zirbel (1997) were judged to generally be the most reliable of the converted values, followed by those of Hill & Lilly (1991) and then those of Yates, Miller & Peacock (1989). Different converted values for the same field that agreed to within their errors were averaged together. Two objects (3C 275 and 3C 435A) have a range of B_{gg} values listed in Table 7 because other studies yielded highly discrepant values and, in the absence of other data, it is unclear which of the values is more reliable in these specific cases.

The distribution of the B_{gg} values listed in Table 7 is shown in Figure 4. The two objects (3C 275 and 3C 435A) with a range of B_{gg} values listed in Table 7 are omitted from Figure 4 and from all further analysis and discussions. Table 7 contains 17 sources with $B_{gg} > 500 \text{ Mpc}^{1.77}$. The richness of all 17 of these fields has been previously noted in one form or another in the literature. Most notably, 3C 28 has the richest environment (excluding the upper limit on the range for 3C 435A) and is a known Abell cluster (Abell 115) and a known X-ray cluster (McCarthy et al. 1995 and references therein). In addition to the references listed in Tables 6 and 7, information on the fields surrounding the remaining sources with $B_{gg} > 500 \text{ Mpc}^{1.77}$ can be found in Wyndham (1966), Kristian, Sandage & Karem (1974, 1978), Hintzen & Stocke (1986), Ellingson et al. (1991b), Spinrad et al. (1991) and references therein, Ellingson et al. (1994), McCarthy et al. (1995), Hall et al. (1995), Rector, Stocke & Ellingson (1997), Hes et al. (1996) and Gizani & Leahy (1999).

5. Results

5.1. Radio Galaxy Environments vs. Quasar Environments

The environments of the two samples must be compared as a function of redshift because EYG have shown that quasar environments vary dramatically with redshift. Figure 5 shows the sample plotted both as a function of redshift and absolute nuclear B magnitude. Sources located in rich environments ($B_{gg} > 500 \text{ Mpc}^{1.77}$) are denoted by filled symbols while those in poor environments ($B_{gg} \leq 500 \text{ Mpc}^{1.77}$) are marked with open symbols. The absolute nuclear B magnitude is in general agreement with the AGN classification; i.e., all quasars have $M_B < -22.5$ while all but 4 of the radio and N-galaxies have $M_B > -22.5$. For consistency, the 4 galaxies with $M_B < -22.5$ are reclassified as quasars for the environment comparisons discussed below (this has no significant effect on the results).

Note the gap in magnitude between the quasars and most of the radio galaxies in Figure 5. It is unclear whether this gap is real or due to possible systematic differences in the way the absolute nuclear B magnitude was calculated for quasars and radio galaxies. Quasars were assumed to have a negligible host galaxy contribution and so a total magnitude was used for the nuclear magnitude. For radio galaxies, a magnitude in the inner 1-2 kpc was used to estimate the nuclear magnitude. The systematic effect of including the host galaxy contribution in the quasar nuclear magnitudes can be estimated using a “typical” AGN host galaxy magnitude of $M_{host_B} = -22$. (estimated from the radio galaxy data in Table 3). Removing such a contribution makes an $M_B = -23$ quasar nuclear magnitude dimmer by 0.6 mag. Thus, the net effect would be to spread out the lower envelope of the quasar nuclear magnitude distribution, but this is insufficient to close the gap in Figure 5 entirely. So it seems possible that some systematic differences in magnitudes could be present. Still, this systematic is not large enough to cause a significant overlap of quasar and radio galaxy absolute nuclear B magnitudes (i.e., few objects would be misclassified).

Also plotted in Figure 5 is a very low z ($z < 0.1$) sample of radio galaxies, taken from YE93, which contains a mixture of FR1 and FR2 type sources (all those at $z < 0.1$ with $B_{gg} > 500 \text{ Mpc}^{1.77}$ are FR1s). Although it has been included on this plot, this sample is NOT included in any comparison between quasar and radio galaxy properties because there are no quasars at this low redshift. Originally, the case for an evolutionary fading model for quasars was made by EYG on the basis of their quasar sample at $z > 0.3$ and this very low z ($z < 0.1$) sample of radio galaxies. The data from the present work fill the ~ 4 Gyr gap between these two samples.

An inspection of just the quasars in Figure 5 shows that there are a substantial number of quasars found in rich environments at $0.4 < z < 0.65$ but there are none found in rich environments at $z < 0.4$. This dramatic result is presented and discussed in EYG and YE93 and is the basis for their evolutionary hypothesis. We choose the $0.15 < z < 0.4$ redshift range in which to compare radio galaxy and quasar environments because of the striking absence of quasars in rich environments at these redshifts. The orientation angle hypothesis of Barthel (1989) predicts that

the percentage of quasars found in rich environments at $0.15 < z < 0.4$ should be the same as the percentage of radio galaxies found in rich environments over that same redshift range. However, a Kolmogorov-Smirnov test yields only a 3% chance that the two distributions of B_{gg} values were drawn from the same parent population (Figure 6). On this basis the orientation angle hypothesis of Barthel (1989) is rejected at the 97% (2.2σ) confidence level.

Since N-galaxies do have a strong point source component, it is possible that N-galaxies are actually quasars with either a slightly lower luminosity AGN or a slightly brighter host galaxy. If the above analysis is redone with *all* N-galaxies grouped together with the quasars (rather than grouping those with $M_B > -22.5$ with the radio galaxies), the difference in the environments of the radio galaxies and quasars at $0.15 < z < 0.4$ becomes even larger: a KS test gives only a 0.4% chance, or a rejection at the 3σ level, that the two distributions come from the same parent population.

Because the AGN nuclear magnitudes are drawn from a continuous luminosity function with a somewhat unclear observational magnitude limit, we follow YE93 and quantify the relative evolution of rich and poor environments by building a model of the brightest AGN one would expect to see, as a function of redshift. We use the two-power-law model of the quasar luminosity function from Boyle et al. (1988), with evolution in the characteristic quasar luminosity parametrized as $L^*(z) = L_0(1+z)^{\kappa_L}$. This luminosity function is used along with the relation for cosmological volume as a function of redshift, to produce a family of curves describing the brightest AGN one would see at any given redshift, for various values of the rate of evolution, κ_L . The curves are normalized empirically to $z \sim 0.6$, where the brightest radio-loud quasars observed in the 3CR sample are often found in rich environments.

In agreement with YE93, we find the “standard model” ($\kappa_L = 3.7$; solid line) to be a good fit to the upper envelope of all the data in Figure 5. This model is based on the well-determined parameters for optically-selected quasars, and hence describes the general population of very luminous AGN, which here are mostly located in poor environments. The model corresponding to $\kappa_L = 19$ (dash-dot line) was found to be the best match for the upper envelope of the data when only the sources in rich environments in Figure 5 (i.e., only the filled symbols) were used.

An upper limit on the e-folding time (τ) for the fading of quasars can be obtained by assuming an exponential form for the luminosity evolution, $L^*(z) = L_0 e^{t/\tau}$. For sources in rich ($B_{gg} > 500 \text{ Mpc}^{1.77}$) environments (i.e., $\kappa_L = 19$) at $z = 0.4$ (the middle of our redshift range), the resulting e-folding time for quasars is 0.9 Gyr for $H_0 = 50, q_0 = 0$ (0.6 Gyr for $H_0 = 75, q_0 = 0$). Comparing the κ_L values of these fits to the upper envelope of the sources in poor ($\kappa_L = 3.7$) and rich ($\kappa_L = 19$) environments, it appears that sources in rich environments evolve ~ 5 times faster than those in poor environments. Changing the B_{gg} value that defines a rich environment from 500 to 400 or 600 $\text{Mpc}^{1.77}$ has little effect on these results. The upper envelope of the sources with $B_{gg} > 400 \text{ Mpc}^{1.77}$ is well fit by the model corresponding to $\kappa_L = 16$ while that of the sources with $B_{gg} > 600 \text{ Mpc}^{1.77}$ is well fit by a $\kappa_L = 24$ curve. The e-folding times associated with these values of κ_L

vary by only $\sim 20\%$ (a 19% increase in τ for $\kappa_L = 16$ and a 21% decrease in τ for $\kappa_L = 24$) from those corresponding to the $\kappa_L = 19$ curve. While changing the definition of a rich environment to $B_{gg} > 700 \text{ Mpc}^{1.77}$ still has little effect on the results (the $\kappa_L = 24$ model is still a good fit to this upper envelope), dropping the limit to $B_{gg} > 300 \text{ Mpc}^{1.77}$ has a drastic effect. In this case, the standard envelope model ($\kappa_L = 3.7$) is a good fit and the e-folding times increase by more than a factor of 5.

Although the evidence presented above makes it very unlikely that the orientation angle hypothesis of Barthel (1989) is the primary means of relating quasars and radio galaxies, it is possible that *some* quasars are radio galaxies with their jet oriented close to our line of sight (within $\sim 45^\circ$). Thus, Barthel's hypothesis may be valid for individual objects but it is almost certainly not valid for the AGN population as a whole. Also, we cannot rule out that quasars and radio galaxies are related to one another by some combination of both evolution and orientation.

5.2. Correlations Between Environment and Other AGN Properties

Since the 3CR sample is flux-limited, the radio power and redshift are highly correlated ($r = 0.65$ at a confidence level $> 99.9\%$). Thus, there is the possibility that the distribution of the objects in rich environments seen in Figure 5 is actually due to a correlation between radio power and environment at a given redshift combined with the radio power-redshift correlation of the 3CR sample. Yates, Miller & Peacock (1989) do find a slight correlation between radio power and environment in their study of radio galaxies, as do Wold et al. (2000). Hill & Lilly (1991), whose study of radio galaxies is well-suited to answer this question because of its large range of radio powers and its relatively narrow redshift range, find no evidence of a correlation between radio power and environment at $z \sim 0.5$.

In Figure 7, the total radio power at 178 MHz of all the 3CR objects used in this study (including the radio galaxies with $z < 0.1$ taken from YE93 which are not part of the present sample) are plotted versus redshift with filled symbols indicating objects with $B_{gg} > 500 \text{ Mpc}^{1.77}$. The symbols have the same meaning as in Figure 5 and quasars with unknown environments are marked with an “X”. A visual inspection of Figure 7 shows that, with a few exceptions, for each object in a rich environment there are objects at a similar redshift in a poor environment with equal or greater radio power (i.e., the objects in rich environments, in general, are not the most powerful radio sources at a given redshift). Ignoring the objects with $z < 0.1$, a correlation analysis using the remaining 3CR objects (i.e., those in the sample of this work) yields a correlation coefficient between radio power and environment of $r = 0.27$ at a confidence level of $\sim 97\%$. Thus, there does appear to be a slight correlation between radio power and environment for the objects in the present sample but not as strong a correlation as would be required to create the apparent evolutionary effect seen in Figure 5.

Figure 8 shows the complete sample, including the quasars which are not 3CR sources. While

a number of these objects lie at somewhat lower radio powers than the radio galaxies at similar redshifts, their powers are still well above many radio galaxies which are located in clusters. The lack of clusters in this sample is thus difficult to explain in a unified model. We note that about 10% of the quasar sample may be core dominated (Rector, Stocke & Ellingson 1997, Hutchings et al. 1998), indicating that their total radio powers may be overestimates of their lobe power. However, these objects are found in both rich and poor environments, suggesting that this does not strongly affect the comparison of radio galaxies and quasars.

Additionally, there is no significant correlation between total M_r (and thus host galaxy M_r) and B_{gg} , although virtually all of these FR2 host galaxies are much more luminous than M^* . Specifically, eight of the nine FR2s with M_r determined and $B_{gg} \geq 500 \text{ Mpc}^{1.77}$ have absolute host luminosities 1-2 mags brighter than M^* (3CR 435.0A is the lone exception with a poorly determined magnitude 0.5 mags less luminous than M^*). These values are typical of poor cluster brightest cluster galaxies (Hoessel, Gunn & Thuan 1980; Wurtz et al. 1997), and, as found by other studies (Lilly & Prestage 1987; Allington-Smith et al. 1993), the radio galaxies are the brightest members of their groups and poor clusters.

Finally, we briefly examined the relationship between the environment and the optical class (column 9 of Table 1) of each source. The distribution of B_{gg} values was found to be similar for all optical classes and no significant difference in the percentage of rich environments ($B_{gg} > 500 \text{ Mpc}^{1.77}$) for each optical class was found. So, based on the correlation analyses discussed above, the behavior illustrated in Figure 5 appears to be genuine and not due to secondary and/or multiple correlations of the various other AGN parameters.

6. Conclusion

6.1. Summary of the Results

The results of this work are summarized below:

1. A comparison of the environments of 51 radio galaxies and 67 quasars in the redshift range $0.15 < z < 0.65$ clearly shows that while quasars are found in rich environments ($B_{gg} > 500 \text{ Mpc}^{1.77}$; i.e., Abell richness class 0 and above) only at $z > 0.4$ (EYG), radio galaxies are found in rich environments over the entire redshift range with the percentage of radio galaxies in rich environments at $0.15 < z < 0.4$ (20%) being comparable to that of radio galaxies in rich environments at $0.4 < z < 0.65$ (28%) and quasars in rich environments at $0.4 < z < 0.65$ (36%). A K-S test gives only a 3% chance that the B_{gg} distributions of the radio galaxies and quasars at $0.15 < z < 0.4$ come from the same parent population. On this basis, the orientation angle hypothesis of Barthel (1989) is rejected at the 97% (2.2σ) confidence level as the primary means of relating quasars and radio galaxies. If all N-galaxies are grouped with the quasars, the hypothesis of Barthel (1989) is rejected at the 99.6% (3σ) confidence level. However, a combination of Barthel's

orientation hypothesis and EYG’s evolutionary hypothesis cannot be ruled out.

2. Applying the evolutionary model (pure luminosity evolution; i.e., no number density evolution) described in YE93, we find that the “standard envelope model” ($\kappa_L = 3.7$) is a good fit to the upper envelope of the sources in poor environments while a model corresponding to $\kappa_L = 19$ matches the upper envelope of the sources in rich ($B_{gg} > 500 \text{ Mpc}^{1.77}$) environments. A comparison of these two values of κ_L implies that sources in rich environments evolve ~ 5 times faster than those in poor environments. Converting κ_L to an e-folding time (τ), the maximum e-folding time for quasars in rich ($B_{gg} > 500 \text{ Mpc}^{1.77}$) galaxy environments is $\tau \sim 0.9 \text{ Gyr}$ for $H_0 = 50, q_0 = 0$ ($\tau \sim 0.6 \text{ Gyr}$ for $H_0 = 75, q_0 = 0$). All these results are in excellent agreement with YE93 and are not strongly dependent upon the exact choice of B_{gg} used to define a rich environment.

3. It is unlikely that the redshift relationship between the radio galaxies in rich environments and the quasars in rich environments seen in Figure 5 is due to a correlation between radio power and environment coupled with the redshift-radio power correlation of the flux-limited 3CR sample. Nor do any other secondary or multiple correlations appear to be responsible.

6.2. A Compatible Hypothesis

In this Section we describe a compatible hypothesis for the results presented here. This hypothesis links the observed evolution of AGN activity in clusters with the decline of individual sources in response to evolution in their cluster environment. While this may not be the only physical mechanism that could account for these results (e.g., systematic changes in jet opening angle with time for AGN in clusters is another possibility), the scenario we propose is simple and consistent with both theoretical ideas about the triggering of quasars and observational constraints on the evolution of the cluster gravitational potential well from X-ray observations. The ideas presented below also are most easily understood in a model by which a single cluster AGN undergoes secular evolution in power, instead of a statistical fading of cluster AGN as a population. While either possibility is consistent with current data, we note that cD galaxies in rich clusters in the current epoch are luminous radio emitters (i.e., typically $\log P_{rad} \geq 25 \text{ W Hz}^{-1}$) 35-40% of the time. So in the case of the cD galaxies, like those in which the quasars and radio galaxies in this study are located, a large fraction of the full population of such objects is radio-loud at any one time, unless the current epoch statistics are very anomalous. Since several lines of argument suggest that single radio source lifetimes are 10^{7-8} yrs, every cD galaxy must have “turned on” several times in the last few Gyrs to account for the current epoch statistics. Therefore, particularly for the cD galaxies, a recurrent outburst hypothesis is particularly attractive, and so we will assume that this idea is correct in the discussion below.

The triggering of quasars is believed to be caused by galaxy-galaxy interactions and mergers (e.g., Roos 1981; Barnes & Hernquist 1992; Wilson & Colbert 1995). However, the rate and relative velocities of these interactions and mergers change as the clustering environment around the

quasar evolves. In the early stages of cluster formation, the duration of galaxy-galaxy interactions tends to be longer because the cluster potential well is still shallow and the galaxies have not yet reached their full orbital speed. In this stage of cluster evolution, mergers are still efficient at destroying disk structures and transferring gas (e.g., Mihos 1995). However, as a cluster virializes and begins to come into dynamical equilibrium, the orbital speeds of the galaxies increase and the galaxy orbits stabilize. Galaxy-galaxy mergers and interactions become less frequent and are of shorter duration, making them less effective at triggering AGN activity (Aarseth & Fall 1980; Roos 1981; Wilson & Colbert 1995).

Several authors (e.g., Blandford & Znajek 1977; Begelman, Blandford & Rees 1980; Wilson & Colbert 1995) have suggested that, unlike radio-quiet AGN, radio-loud AGN are powered by the spin energy extracted from very rapidly spinning supermassive black holes (SMBHs). Rapidly spinning SMBHs can be formed most easily from the capture and subsequent orbital evolution of a SMBH binary system (on a timescale of 10^8 yrs after the binary pair is formed; but see Begelman, Blandford & Rees (1980) who advocate much longer timescales). Under certain circumstances, merging disk galaxies can provide non-rotating SMBHs from their nuclei (Wilson & Colbert 1995) and the eventual merger of the SMBH pair forms the very rapidly spinning SMBH, whose spin energy is extracted by the Blandford-Znajek mechanism to create the radio jets and other radio-loud quasar manifestations. As the cluster virializes, the absence of suitably slow encounters prevents the formation of new SMBH binaries as well as the injection of mass into the region of the SMBH. Thus, the existing SMBH can only spin down as it releases energy, creating lower power outbursts over time; i.e., a luminous quasar at $z \sim 0.5$ fades to become an FR2 radio galaxy then an FR1 radio galaxy. In this picture, the fading timescale of 0.9 Gyrs found by this work is the spin down time for the SMBH.

Alternately, the quasar is starved of fuel as the cluster virializes. The nuclear engine of the quasar (i.e., the AGN) is believed to be fueled by gas from either the quasar host galaxy or from an interacting companion galaxy (Roos 1981, 1985; De Robertis 1985). In the early stages of cluster formation, galaxies are believed to contain an abundance of gas and so fuel for the AGN is plentiful. However, as a cluster develops, an intracluster medium (ICM) begins to form due to the combined remnants of galaxy-galaxy interactions and mergers (e.g., tidal tails). As the ICM becomes dense ($> 10^{-4} \text{ cm}^{-3}$), it will begin to strip or “sweep” gas out of the galaxies moving through it (Stocke & Perrenod 1981), making itself more dense and even more effective at “sweeping” gas (Gisler 1976). As the gas sweeping ability of the ICM increases, potential fuel for the AGN is more easily stripped from cluster galaxies moving through the medium and heated to X-ray emitting temperatures. This positive feedback loop may eventually starve the AGN (by decreasing the gas reservoir in both the AGN host galaxy and the interacting companion galaxies) causing it to dim.

In this scenario, therefore, the evolution of the fraction of AGN seen in clusters probes the systematic evolution of the physical conditions within the cluster environment. Because of their sensitivity to local conditions, the most optically luminous AGN mark primarily poor groups *or* those richer systems which are in the early stages of virilization. Thus, clusters of a given richness

will no longer harbor quasars past a certain epoch. For clusters having a richness of $B_{gg} \sim 500$ Mpc^{1.77}, this epoch is $z \sim 0.4$ (EYG). This quasar dimming will occur at an earlier epoch for even richer environments than those discovered here (i.e., Abell richness class 2 and higher) while for poorer environments it will occur closer to the present time. That is, to our knowledge, no quasar or luminous radio galaxy (i.e., FR2) has been discovered in an *extremely* rich cluster ($B_{gg} > 1500$ Mpc^{1.77}) at $z < 0.65$. The scenario described here suggests that this absence occurs because the ICM in extremely rich clusters is already too dense and quasars therein have been “starved” at earlier epochs. Thus, by $z \sim 0.6$ these AGN have faded through luminous FR2 radio galaxies to become low power FR1 radio galaxies. The study of radio sources in the richest cluster environments ($B_{gg} > 1500$ Mpc^{1.77}) at $z = 0.3 - 0.8$ by Stocke et al. (1999) supports this suggestion, finding only FR1 type sources in these clusters.

The maximum evolutionary e-folding time of ~ 0.9 Gyr is a factor of several shorter than the virialization timescale for the entire cluster; however, quasar evolution is more likely to be affected by the conditions in the cluster core region, rather than the 1 Mpc scale environment. Thus, even if cluster virialization triggers the fading of these quasars, the fading itself occurs too rapidly to be “tracking” the subsequent cluster evolution. However, evolution of the cluster core could “track” quasar fading. Assuming a cluster core radius of 0.1 - 0.25 Mpc (based on the extent of X-ray emission from clusters; Henry et al. 1992) and 5 crossing times for virialization, the virialization time of a cluster core would be $\sim 1 - 2.5$ Gyr which is more comparable to the quasar fading time we find above. Therefore, while cluster virialization initially “starves” the quasar by one or both of the mechanisms above, the actual fading timescale must be due to some internal AGN clock, not to any timescale in the larger environment of the AGN, all of which are too long.

6.3. Further Tests of This Hypothesis

Additional studies can test some of the ideas proposed in this work. Based on the scenario presented above, clusters of richness $B_{gg} \gtrsim 500$ Mpc^{1.77} at $z > 0.4$ hosting AGN would be expected to have lower velocity dispersions and higher fractions of blue, star-forming galaxies than clusters of similar richness at $z < 0.4$ (e.g., Ellingson et al. 1994). The link between ICM and AGN activity would suggest that AGN-hosting clusters of richness $B_{gg} \gtrsim 500$ Mpc^{1.77} at $z < 0.4$ have a denser ICM than clusters of similar richness at $z > 0.4$; Hall et al. (1995) show that extended X-ray luminosities around quasars fall in the lower range of what is expected from clusters of similar richness. A more conclusive test of this hypothesis could be performed using sensitive, high resolution X-ray images such as those from ACIS aboard Chandra to search for direct detections of a dense, hot ICM surrounding both the quasars and radio galaxies at $z < 0.4$. An indirect investigation of the ICM surrounding the sources studied here using the extended radio morphology of these sources is presented in Paper 2; the results support this hypothesis and suggest that a dense ICM can affect extended radio structure and may even cause FR2 type radio sources to evolve into FR1-like structures at $z < 0.4$.

We wish to thank KPNO for telescope time and support given to us for this project. M.H. acknowledges the support of a NASA Graduate Student Research Program Fellowship NGT - 51291 and the travel support of NOAO to conduct these thesis observations. EE would like to acknowledge NSF grant AST-9617145. H.K.C. Yee is thanked for the use of his PPP program and for numerous helpful discussions. G. Hill is also thanked for his cooperation. This research has made use of the NASA/IPAC Extragalactic Database (NED) which is operated by the Jet Propulsion Laboratory, California Institute of Technology, under contract with NASA.

REFERENCES

Aarseth, S.J., & Fall, S.M. 1980, *ApJ*, 236, 43

Abell, G.O. 1958, *ApJS*, 3, 211

Allington-Smith, J.R., Ellis, R.S., Zirbel, E.L., & Oemler, A. 1993, *ApJ*, 404, 521

Baars, J. W. M., Genzel, R., Pauliny-Toth, I. I. K., & Witzel, A. 1977, *A&A*, 61, 99

Barnes, J.E., & Hernquist, L. 1992, *ARA&A*, 30, 705

Barthel, P.D. 1989, *ApJ*, 336, 606

Begelman, M.C., Blandford, R.D., & Rees, M. J., 1980, *Nature*, 287, 307

Bennett, A.S. 1962, *MmRAS*, 68, 163

Blandford, R.D., & Znajek, R.L. 1977 *MNRAS*, 179, 433

Boyle, B.J., Shanks, T., & Peterson, B.A. 1988, *MNRAS*, 235, 935

Burstein, D., & Heiles, C. 1982, *AJ*, 87, 1165

Cardelli, J.A., Clayton, G.C., & Mathis, J. S. 1989, *ApJ*, 345, 245

de Koff, S., Baum, S.A., Sparks, W.B., Biretta, J., Golombek, D., Macchetto, F., McCarthy, P., & Miley, G.K. 1996, *ApJS*, 107, 621

De Robertis, M. 1985, *AJ*, 90, 998

de Vaucouleurs, G. 1948, *Ann. d'Astrophys.*, 11, 247

Ellingson, E., Yee, H.K.C., Bechtold, J., & Dobrzański, A. 1994, *AJ*, 107, 1219

Ellingson, E., Yee, H.K.C., & Green, R.F. 1991a, *ApJ*, 371, 49 (EYG)

Ellingson, E., Yee, H.K.C., & Green, R.F. 1991b, *ApJS*, 76, 455

Fanaroff, B.L., & Riley, J.M. 1974, *MNRAS*, 167, 31P

Feigelson, E.D., & Berg, C.J. 1983, *ApJ*, 269, 400

Fukugita, M., Shimasaku, K., & Ichikawa, T. 1995, *PASP*, 107, 945

Giovannini, G., Feretti, L., Gregorini, L., & Parma, P. 1988, *A&A*, 199, 73

Gisler, G.R. 1976, *A&A*, 51, 137

Gizani, N.A.B., & Leahy, J.P. 1999, *New Astronomy Reviews*, 43, 639

Gower, J. F. R., Scott, P. F., & Wills, D. 1967, MmRAS, 71, 49

Hall, P., Ellingson, E., & Green, R.F. 1995, AJ, 113, 1179

Hardcastle, M.J., Alexander, P., Pooley, G.G., & Riley, J.M. 1997, MNRAS, 288, 859

Harvanek, M., & Stocke, J.T., 2001, in prep. (Paper 2)

Heckman, T.M., Smith, E.P., Baum, S.A., van Breugel, W.J.M., Miley, G.K., Illingworth, G.D., Bothun, G.D., & Balick, B. 1986, ApJ, 311, 526

Hes, R., Barthel, P.D., & Fosbury, R.A.E. 1996, A&A, 313, 423

Hill, G.J., & Lilly, S.J. 1991, ApJ, 367, 1 (HL)

Hintzen, P., & Stocke, J. 1986, ApJ, 308, 540

Hoessel, J.G., Gunn, J.E., & Thuan, T.X. 1980, ApJ, 241, 486.

Hutchings, J., B. 1987, ApJ, 320, 122

Hutchings, J. B., Dewey, A., Chaytor, D., Ryneveld, S., Gower, A. C., & Ellingson, E. 1998, PASP, 110, 111

Jackson, N., & Rawlings, S. 1997, MNRAS, 286, 241

Kellermann, K. I., Pauliny-Toth, I. I. K., & Williams, P. J. S. 1969, ApJ, 157, 1

Kent, S.M. 1985, PASP, 97, 165

King, C.R., & Ellis, R.S. 1985, ApJ, 288, 456

Kristian, J., Sandage, A., & Katem, B. 1974, ApJ, 191, 43

Kristian, J., Sandage, A., & Katem, B. 1978, ApJ, 219, 803

Laing, R. A., & Peacock, J. A. 1980, MNRAS, 190, 903

Laing, R. A., Riley, J. M., & Longair, M. S. 1983, MNRAS, 204, 151

Lilly, S.J., & Prestage, R.M. 1987, MNRAS, 225, 531

Longair, M.S. 1985, in Radio Astronomy and the Physics of the Universe, ed. R. Fanti, G. Grueff, & G. Setti (Bologna: Istituto di Radioastronomia del CNR), 25

Longair, M.S., & Seldner, M. 1979, MNRAS, 189, 433

McCarthy, P.J., Spinrad, H., & van Breugel, W. 1995, ApJS, 99, 27

McCarthy, P.J., van Breugel, W., & Spinrad, H. 1989, AJ, 97, 36

Mihos, J.C. 1995, ApJ, 438, L75

Miley, G. 1980, ARA&A, 18, 165

NASA/IPAC Extragalactic Database 1997, Internet WWW page, at URL:
<<http://nedwww.ipac.caltech.edu/NED.html>>

Owen, F.N. 1986, in IAU Symp. 119, Quasars, ed. G. Swarup & V.K. Kapahi (Dordrecht: Reidel), 173

Pilkington, J. D. H., & Scott, P. F. 1965, MmRAS, 69, 183

Prestage, R.M., & Peacock, J.A. 1988, MNRAS, 230, 131

Prestage, R.M., & Peacock, J.A. 1989, MNRAS, 236, 959

Rector, T., Stocke, J.T., & Ellingson, E. 1995, AJ, 110, 1492

Roos, N. 1981, A&A, 104, 218

Roos, N. 1985, ApJ, 294, 479

Sebok, W.L. 1986, ApJS, 62, 301

Seldner, M., & Peebles, P.J.E. 1978, ApJ, 225, 7

Smith, E.P., Heckman, T.M., Bothun, G.D., Romanishin, W., & Balick, B. 1986, ApJ, 306, 64

Smith, H.E., Spinrad, H., & Smith, E.O. 1976, PASP, 88, 621

Spinrad, H., Djorgovski, S., Marr, J., & Aguilar, L. 1985, PASP, 97, 932

Spinrad, H., et al. 1991, electronic version of The Revised 3C Catalog of Radio Sources.

Stocke, J.T., Perlman, E.S., Gioia, I.M., & Harvanek, M. 1999, AJ, 117, 1967

Stocke, J.T., & Perrenod, S.C. 1981, ApJ, 245, 375

Stockton, A., & MacKenty, J.W. 1987, ApJ, 316, 584

Tadhunter, C. N., Morganti, R., di Serego-Alighieri, S., Fosbury, R. A. E., & Danziger, I. J. 1993, MNRAS, 263, 9

Wilson, A.S., & Colbert, E.J.M. 1995, ApJ, 486, 62

Wold, M., Lacy, M., Lilje, P.B., & Serjeant, S. 2000, MNRAS, 316, 267

Worrall, D.M. 1987, in Superluminal Radio Sources, ed. J.A. Zensus and T.J. Pearson (Cambridge: Cambridge University Press), 251

Wurtz, R., Stocke, J.T., Ellingson, E., & Yee, H.K.C. 1997, ApJ, 480, 547

Wyndham, J.D. 1966, ApJ, 144, 459

Yates, M.G., Miller, L., & Peacock, J.A. 1989, MNRAS, 240, 129 (YMP)

Yee, H.K.C. 1991, PASP, 103, 396

Yee, H.K.C., & Ellingson, E. 1993, ApJ, 411, 43 (YE93)

Yee, H.K.C., Ellingson, E., & Carlberg, R. G. 1996, ApJS, 102, 269

Yee, H.K.C., & Green, R.F. 1984, ApJ, 280, 79

Yee, H.K.C., & Green, R.F. 1987, ApJ, 319, 28 (YG)

Yee, H.K.C., Green, R.F., & Stockman, H.S. 1986, ApJS, 62, 681

Yee, H.K.C., & López-Cruz, O. 1999, AJ, 117, 1985

Zamorani, G., et al. 1981, ApJ, 245, 357

Zirbel, E.L. 1997, ApJ, 476, 489

Fig. 1.— The data points with 1σ error bars and the weighted linear fit that is the conversion from Zirbel (1997) “richness” values ($N_{0.5}^{-19}$) to B_{gg} . The fit has been forced through the point (0,0). The resulting conversion is $B_{gg} = 38N_{0.5}^{-19}$.

Fig. 2.— The data points with 1σ error bars and two possible fits for the conversion from Yates, Miller & Peacock (1989; YMP) B_{gg} values to our B_{gg} values. The solid line is the conversion based on the average offsets of the data points (i.e., a forced slope of unity). The dashed line is a weighted least squares linear fit. The two fits agree to within their errors. The two uppermost data points were not used in the calculation of either fit (for reasons given in the text). The average offset fit (the solid line; $B_{gg} = \text{YMP } B_{gg} + 70$) was used for the conversion.

Fig. 3.— The data points with 1σ error bars and the weighted linear fit that is the conversion from Hill & Lilly (1991; HL) $N_{0.5}^M$ values to B_{gg} . The fit has been forced through the point (0,0). The resulting conversion is $B_{gg} = 33N_{0.5}^M$. This fit agrees quite well with the conversions discussed in HL.

Fig. 4.— A histogram showing the distribution of B_{gg} values. The open blocks are the radio galaxies and N-galaxies; the shaded blocks are the quasars. The two objects with a very large discrepancy between B_{gg} values found by other investigations (3C 275 and 3C 435A) are not included in the distribution.

Fig. 5.— Nuclear M_B vs. z for radio galaxies, N-galaxies and quasars. The absolute magnitudes are in rest-frame Johnson B and have been corrected for Galactic reddening. The radio galaxies appear as diamonds, the N-galaxies as triangles and the quasars as squares. Sources that are located in rich environments ($B_{gg} > 500 \text{ Mpc}^{1.77}$) are denoted by filled symbols while those in poor environments ($B_{gg} \leq 500 \text{ Mpc}^{1.77}$) are marked with open symbols. For some sources the environment is unknown and these are marked with either an asterisk (radio galaxies) or a plus sign (N-galaxies). Symbols with an arrow indicate that the absolute nuclear B magnitude is an upper limit. The $z = 0.15 - 0.65$ radio and N-galaxies are from the present work, the lower redshift galaxies are from Yee & Ellingson (1993) and the quasars are originally from Ellingson, Yee & Green (1991; EYG). Model curves for the upper envelope of the points are derived from an AGN luminosity function, using a “standard $\kappa_L = 3.7$ model” (solid line), matching the upper envelope for all objects, and a $\kappa_L = 19$ model (dot-dashed line) describing the upper envelope for the quasars and radio galaxies in rich environments (see text for details).

Fig. 6.— a) The distribution of B_{gg} values for the galaxy environments of radio galaxies and N-galaxies with $0.15 < z < 0.4$. The N-galaxies are the shaded blocks. b) The distribution of B_{gg} values for the galaxy environments of quasars with $0.15 < z < 0.4$. A KS-test gives only a 3% chance that these two distributions come from the same parent population. If the N-galaxies are grouped with the quasars, the probability is 0.4%.

Fig. 7.— Total P_{178} vs. z for all 3CR objects (both galaxies and quasars) used in this study (including the radio galaxies with $z < 0.1$ taken from Yee & Ellingson 1993). The radio power is the total power emitted in the rest frame at 178 MHz. The symbols have the same meaning as in Figure 5. Two additional quasars with unknown environments are marked with an “X”.

Fig. 8.— Same as Figure 7, but includes all objects in the combined radio galaxy and quasar samples.

A Study of 3CR Radio Galaxies from $z = 0.15$ to 0.65 . I. Evidence for an Evolutionary Relationship Between Quasars and Radio Galaxies

Michael Harvanek^{1,2}, E. Ellingson², & John T. Stocke²

*Center for Astrophysics and Space Astronomy, CB 389 University of Colorado, Boulder, Colorado, 80309-0389,
electronic mail: harvanek, stocke, e.elling@casa.colorado.edu*

and

George Rhee²

*Physics Department, University of Nevada, Las Vegas, NV, 89195
electronic mail: grhee@dawg.physics.unlv.edu*

ABSTRACT

Deep optical images have been gathered for a nearly complete sample of radio galaxies from the Revised 3rd Cambridge (3CR) Catalog in the redshift range $0.15 < z < 0.65$. Total and nuclear magnitudes and colors have been extracted. The richness of the galaxy clustering environment has also been quantified by calculating the amplitude of the galaxy-galaxy spatial covariance function (B_{gg}), showing overdensities ranging up to Abell class 0-1 clusters. These optical data are compared to similar data from an existing sample of radio-loud quasars in the same redshift range for the purpose of determining the relationship between radio galaxies and quasars. In the range $0.15 < z < 0.4$, we find that quasars and radio galaxies have significantly different environments in that only radio galaxies are found in rich cluster environments. This comparison appears to rule out the hypothesis that all quasars are radio galaxies viewed from a particular angle at the 97% confidence level (99.6% confidence level if N -galaxies are considered quasars). The existence of quasars in clusters at $z > 0.4$ supports the hypothesis that some radio-loud quasars may dim with time and evolve into radio galaxies with an e-folding time of ~ 0.9 Gyr. A compatible scenario is presented for this evolution in which the quasar dims due to the absence of low velocity interactions between the quasar host and companion galaxies which trigger quasar activity and/or a diminishing fuel supply caused by the more effective gas “sweeping” of a growing intracluster medium.

¹Current Address: Apache Point Observatory, 2001 Apache Point Rd., PO Box 59, Sunspot, NM, 88349-0059,
email: harvanek@apo.nmsu.edu

²Visiting Astronomer, Kitt Peak National Observatory, National Optical Astronomy Observatories, which is operated by the Association of Universities for Research in Astronomy, Inc. (AURA) under cooperative agreement with the National Science Foundation.

Subject headings: galaxies: active — galaxies: clusters: general — galaxies: evolution — galaxies: nuclei — galaxies: photometry — quasars: general

1. Introduction

Radio galaxies are one of the many types of active galactic nuclei (AGN) recognized today. Currently, the list of AGN types includes quasars, QSOs, radio galaxies (broad and narrow lined), Seyfert galaxies (types I and II) and blazars. The observational properties of the different types of AGN vary considerably, and although all are thought to be driven by a supermassive ($> 10^6$ solar mass) black hole at the nucleus of their host galaxy, the relationships among the various types of AGN are not well understood. The currently accepted model for radio-loud AGN invokes a supermassive black hole that powers a relativistic jet, creating Doppler-boosted, beamed radiation. Differences in the amount of obscuration of the AGN, orientation of the jet with respect to the line of sight, motion of the jet, properties of the black hole and evolution have all been used in various combinations to explain the differences in the properties of the various AGN types. However, to date, no one model has been able to explain them all. In fact, the “unification” of this diverse group of objects is currently one of the primary goals of extragalactic astronomy.

In an effort to further explore the unification of AGN, this work will examine one of the more controversial AGN relationships: that between quasars and radio galaxies. The radio sources associated with quasars are generally quite similar in both luminosity and morphology to the radio sources associated with the more powerful radio galaxies; typically, both are Fanaroff-Riley Type 2, or FR2, sources (Fanaroff & Riley 1974). Some differences in the radio properties do exist however. Radio galaxies have, on average, weaker radio cores (Miley 1980, Owen 1986), exhibit weaker radio jets (Owen 1986), and can have larger linear dimensions (Miley 1980) than quasars. The spectra of quasars are characterized by broad emission lines. The spectra of a few radio galaxies show broad emission lines while most show only narrow emission lines.” Quasars are luminous in X-rays (e.g., Zamorani et al. 1981; Worrall 1987) whereas radio galaxy AGN are comparatively dim (e.g., Feigelson & Berg 1983). While many are found in elliptical host galaxies, a significant number of quasars (Smith et al. 1986; Hutchings 1987; Stockton & MacKenty 1987) and powerful radio galaxies (Heckman et al. 1986; Hutchings 1987; de Koff et al. 1996) are found in hosts with peculiar optical morphologies, indicating interacting and/or merging systems. Finally, more luminous quasars and radio galaxies (e.g., those from the 3CR catalogs of Laing et al. (1983) and Spinrad et al. (1991)) have remarkably similar redshift distributions at $z \gtrsim 0.4$ (Longair 1985; Barthel 1989). All these various relationships between quasars and radio galaxies, along with their differing projected physical sizes and optical polarization properties (see Barthel (1989) and references therein) and evidence for the preferred orientation of some quasars led Barthel (1989) to propose that quasars and FR2 type radio galaxies are the same type of object viewed from a different orientation angle. Since their properties suggest that quasars are beamed toward us, this hypothesis proposes that quasars are FR2 type radio galaxies with their jets oriented closer to our

line of sight (within $\sim 45^\circ$).

However, the work of Yee & Green (1987, hereafter YG), Ellingson, Yee & Green (1991a, hereafter EYG) and Yee & Ellingson (1993, hereafter YE93) suggests another possibility. These studies indicate that while up to one third of optically bright, radio-loud quasars at $z \sim 0.6$ are found in Abell class 0 or richer clusters, a much smaller fraction of lower redshift quasars are found in rich environments. In addition, they found that the brightest quasars which inhabit clusters at $z \sim 0.4$ are several magnitudes fainter than quasars in clusters at higher redshifts. The only radio-powerful AGN found in clusters at low redshifts are radio galaxies. In contrast, the fraction and luminosity of the brightest quasars in poorer environments change relatively little over these epochs. This suggests that environment strongly affects quasar evolution, and that quasars are rapidly disappearing from rich clusters over this redshift range. Based on their findings, EYG proposed that quasars may dim with time and eventually fade to become radio galaxies. This will be referred to as the evolutionary hypothesis of EYG. Note that this hypothesis is not wholly inconsistent with the beaming phenomenon—only with viewing angle being the *sole* explanation for the different AGN classes. In the evolutionary hypothesis, the nuclear properties of some individual objects may be affected by beaming, but there is also a fundamental evolutionary connection between luminous quasars and radio galaxies.

One key to testing these competing hypotheses is the galaxy environments of the FR2 radio galaxies. Assuming that the richness of the galaxy environment is independent of the orientation angle to the line of sight (i.e., the cluster richness remains the same regardless of the angle from which it is viewed), if quasars and FR2 radio galaxies are the same type of object viewed from a different angle, the galaxy environments of quasars and FR2 radio galaxies at the same redshift should be similar. EYG found essentially no optically bright quasars in clusters at $0.15 < z < 0.4$; thus, the orientation angle hypothesis of Barthel (1989) predicts that no FR2 radio galaxies in this redshift range should be found in clusters. However, if quasars evolve into radio galaxies, the galaxy environments of radio galaxies at $0.15 < z < 0.4$ should be similar to that of quasars at some earlier epoch. Since EYG found quasars in both rich and poor environments at $z > 0.4$, their evolutionary hypothesis predicts that the percentage of FR2 radio galaxies found in rich environments at $0.15 < z < 0.4$ should be similar to the percentage of quasars found in rich environments at some epoch $z > 0.4$.

However, consistent data on the galaxy environments of FR2 radio galaxies at $0.15 < z < 0.4$ has been lacking. Although a number of studies of the environments of radio galaxies have been conducted previously (Lilly & Prestage 1987; Prestage & Peacock 1988; Yates, Miller & Peacock 1989; hereafter YMP, Hill & Lilly 1991; hereafter HL; Allington-Smith et al. 1993; Zirbel 1997), much of the data collected were for radio galaxies at higher or lower redshifts. (Note that data for radio galaxies at $z < 0.15$ are abundant. However, since quasars are not found at $z < 0.15$, this data cannot be used to test Barthel's hypothesis.) The studies that did provide adequate coverage over the relevant redshift range (Allington-Smith et al. 1993; Zirbel 1997) used different filters and quantified the richness of the galaxy environment in a somewhat different manner.

Thus, we obtained deep optical images of a sample of 39 radio-powerful 3CR AGN in this redshift range to determine the properties of the AGN nuclear sources and their environments. In Section 2 the radio galaxy and quasar samples are presented. The observations, reductions, photometry and other data processing are discussed in Section 3. In Section 4 the B_{gg} parameter, which quantifies the richness of the clustering environment, is presented in some detail. Incorporation of other clustering data is discussed and the environmental data is tabulated. In Section 5 the properties of the radio galaxies are compared to the properties of quasars and the results of this comparison are used to determine whether the orientation angle hypothesis of Barthel (1989) or the evolutionary hypothesis of EYG can better explain the relationship between quasar and radio galaxy environments. A summary of the results is given in Section 6 and a scenario which accounts for them is proposed. Values of $H_0 = 50 \text{ km s}^{-1} \text{ Mpc}^{-1}$ and $q_0 = 0$ (or 0.02) are assumed throughout this work for consistency with EYG. In a companion paper (Harvanek & Stocke 2001, Paper 2 hereafter) we study the extended radio structure of the sources in this sample.

2. The Samples

2.1. The Observed Sample

The sample chosen for this study was drawn from the 3CR radio galaxies and quasars with $0.15 < z < 0.65$ and $|b| \geq 15^\circ$ that are listed in the Revised 3C Catalog of Radio Sources of Smith, Spinrad & Smith (1976) as updated by Spinrad et al. (1985) and Spinrad et al. (1991). This catalog was chosen as the source of our sample for several reasons. Having originated from the 3CR radio catalog (a list of more than 300 of the brightest radio sources observed at 178 MHz by Bennett (1962)), this catalog ensures that any source at $z > 0.15$ chosen from it will be comparable in radio power to the sources in the quasar comparison sample of YE93 (see below). Furthermore, since the catalog is nearly complete (for sources having 178 MHz flux ≥ 10.9 Jy on the scale of Baars et al. (1977)) and almost entirely identified ($> 91\%$; Spinrad et al. (1991), and objects with $|b| \geq 15^\circ$ are essentially 100% complete) it provides a very comprehensive listing of such sources. Choosing sources from only one flux-limited catalog also helps ensure a uniform sample. The galactic latitude was restricted because the large number of stars and the possibility of uneven extinction near the galactic plane make the measurement of the galaxy environment more uncertain.

Table 1 shows the sample taken from the 3CR catalog and tabulates some of the more useful properties. There are 66 radio galaxies and 14 quasars listed. However, one of the galaxies, 3C 258, was discovered to contain what is believed to be a distant background quasar in its spectrum (A. Dey, private communication). Since the angular size of 3C 258 is quite small for a source at a redshift of $z = 0.165$, it is likely that the radio source is associated with the background object. Thus, this object has been removed from the sample and is excluded from any of the analysis presented in this study.

Listed in Table 1 along with the sources are their optical positions, redshifts, 178 MHz flux

densities on the scale of Baars et al. (1977), and spectral indices between 178 and 750 MHz. (The spectral index α is defined here in the sense $S \propto \nu^{-\alpha}$.) The optical positions and redshifts were taken from Spinrad et al. (1991) except for the optical positions of 3C 225B and 3C 435A, which were taken from Giovannini et al. (1988) (from the cross on the radio map) and McCarthy, van Breugel, & Spinrad (1989), respectively. The 178 MHz flux densities were taken from Laing et al. (1983) if available. If not available in Laing et al. (1983), the values given in Kellermann et al. (1969) were used for most other sources. The 178 MHz flux densities for 3C 99, 3C 258, and 3C 306.1 were taken from Gower et al. (1967) and that for 3C 268.2 was taken from Pilkington & Scott (1965) (all available from the NASA/IPAC Extragalactic Database, 1997) because their values in Kellermann et al. (1969) are likely contaminated by nearby sources. The guidelines for choosing the most appropriate 178 MHz flux density for any given source are discussed in detail in Laing et al. (1983). All fluxes were adjusted to the scale of Baars et al. (1977) using the corrections given in Laing & Peacock (1980). Spectral indices were computed using the 178 MHz flux densities given here and 750 MHz flux densities from Kellermann et al. (1969). Comparison of our spectral index values to those of Laing et al. (1983) shows perfect agreement for all 48 objects common to both samples. For one source, 3C 435A, the 178 MHz flux density and the spectral index were not directly available because the separation of 3C 435 into the two unrelated sources, 3C 435A and 3C 435B, occurred after the work of Kellermann et al. (1969) and we were unable to find these values in more current literature. Since no other data were available, the spectral index of 3C 435A listed in Table 1 is that of the combined source, 3C 435. The 178 MHz flux density was computed using the 1500 MHz flux density of 3C 435A from McCarthy, van Breugel, & Spinrad (1989) and a spectral index for the combined source calculated from fluxes at the appropriate frequencies taken from Kellermann et al. (1969).

Also included in Table 1 are the rest frame luminosity (i.e., power) at 178 MHz, the log of this rest frame luminosity, the optical spectral type of the source (i.e., the “optical class”) and the object type of the source. The rest frame luminosity was calculated from the 178 MHz flux density, the spectral index and the redshift, assuming a Friedmann cosmology with $H_0 = 50 \text{ km s}^{-1} \text{ Mpc}^{-1}$ and $q_0 = 0$. All sources in this sample have a rest frame luminosity above (most well above) the nominal boundary between FR1 and FR2 type radio sources (Fanaroff & Riley 1974). The radio morphology of these sources mostly confirms this FR2 luminosity classification (see also Paper 2 for a more detailed analysis and discussion). The same is true of the quasar comparison sample of YE93 discussed below. We classify each object as “broad-line” (B), “narrow-line” (N) or “low-excitation” (E). Except for 3C 234 and 3C 381, the optical type was taken directly from Jackson & Rawlings (1997) who use a slightly different notation than that used here. Their “quasar/weak quasar” (Q/WQ) classification is equivalent to our broad-line (B) type. Similarly, their “high-excitation galaxy” (HEG) corresponds to our narrow line (N) type and their “low-excitation galaxy” (LEG) is the low-excitation (E) type. The references for the optical spectra on which these classifications are based can be found in Jackson & Rawlings (1997). The optical type for 3C 234 and 3C 381 was taken from Hardcastle et al. (1997) who also provide the references for the optical spectra from which these classifications are determined. The object types are galaxy (GAL), N-galaxy (N) and

quasar (QSO) and were taken directly from Spinrad et al. (1991).

2.2. The Quasar Comparison Sample

For the comparison study, we have utilized the quasar sample of YE93 which contains 65 quasars with $z < 0.65$ and $|b_{II}| \geq 30^\circ$, of which 10 are 3CR sources and most of the remainder are from the 4C and Parkes catalogs. Values of redshift, absolute nuclear B magnitude and B_{gq} (quasar-galaxy two point correlation function amplitudes; see Section 4) are provided by YE93 and for the comparison study we adopt their values directly. When combined with the 3CR sample discussed above, there are a total of 69 quasars and 65 radio galaxies in this study.

3. Observations and Reductions

All optical imaging data were obtained at the 0.9 m and 2.1 m telescopes of the National Optical Astronomy Observatories (NOAO) at the Kitt Peak National Observatory (KPNO). The lower z subsample ($0.15 < z < 0.35$) was observed with the smaller telescope (FOV $\sim 23'$ on a side) while the higher z subsample ($0.35 < z < 0.65$) was observed with the larger telescope (FOV $\sim 5'$ on a side).

The optical observations are listed in Table 2. The Gunn r and Gunn g filters were used for the observations because they match those of the background galaxy counts (Yee et al. 1986, as updated by H. Yee, private communication) and allow for a direct comparison with the quasar work. The integration times are typically 1800 sec in r and 3600 sec in g to yield a completeness magnitude 2-3 mags dimmer than M^* ($M_r^* \sim -22.0$; the combination of k-correction plus moderate luminosity evolution keeps this value approximately constant over the redshift range of interest.) The 5σ limiting magnitude for each field is listed in Table 2. The completeness magnitude is estimated to be ~ 0.8 mag brighter than the 5σ limiting magnitude (Yee, Ellingson & Carlberg 1996).

The identification and classification of all objects in each field and the calculation of an instrumental magnitude for each object were performed using the Picture Processing Package (PPP) software developed by Yee (1991), and further described in Yee, Ellingson & Carlberg (1996). To calibrate the photometry, standard stars from Kent (1985) were observed at several different times during each night of each of the observing runs. Observational uncertainties are typically 0.03-0.1 mag. The observed total apparent magnitudes were corrected for Galactic reddening by using (A_λ/A_V) given by Cardelli, Clayton & Mathis (1989) with the currently accepted value of $R_V = 3.1 \pm 0.1$ and values of $E(B-V)$ for each field taken from Burstein & Heiles (1982). Gunn r absolute magnitudes were k-corrected using the values given in Sebok (1986) for E/S0 type galaxies as a function of z and Gunn g magnitudes were corrected using the tables from Fukugita et al. (1995). Total magnitudes (apparent and absolute) and observed $g-r$ colors for the radio

galaxies are given in Table 3. Those for the quasars are found in Table 4.

Total magnitudes marked with a colon were not obtained from our data. They are estimates based on the brighter of m and m_{15} (total magnitude and magnitude inside 15 kpc, respectively) given in de Koff et al. (1996). These magnitudes were obtained with the Hubble Space Telescope (HST) using the broad-band F702W filter and were converted to Gunn r using the conversions given in Fukugita et al. (1995) for E type galaxies as a function of z . Due to low exposure times and the combination of the extremely high resolution and small pixel size of HST, the magnitudes taken from de Koff et al. (1996) may be dimmer than the actual total magnitudes and so entries marked with a colon in Table 3 should be used with caution.

To estimate the nuclear magnitudes for the radio galaxies, we used m_1 (the magnitude within a 1 kpc radius for $H_0 = 75 \text{ km s}^{-1} \text{ Mpc}^{-1}$, $q_0 = 0.5$, which corresponds to 0.2-0.36" for this redshift range) from de Koff et al. (1996), appropriately corrected to obtain M_B for $H_0 = 50 \text{ km s}^{-1} \text{ Mpc}^{-1}$, assuming a typical power-law AGN spectrum with $\alpha = -0.5$ (YE93), equivalent to a $g - r$ color of -0.11 mag. However, these m_1 magnitudes will contain a small contribution from the host galaxy, although the exact amount is unknown without a detailed knowledge of the inner surface brightness profile. If a deVaucouleurs profile (de Vaucouleurs 1948) is assumed, the galaxy contribution will be typically a few tenths of a mag at most. Therefore, we have used m_1 mags as an estimate of the nuclear magnitudes for all those galaxies in Table 1 whose optical class is N or B. For N or B class radio galaxies, ground-based spectra through apertures considerably larger than 1 kpc are dominated by non-thermal continuum. Additionally, a visual inspection of the spectra in Tadhunter et al. (1993) for those galaxies in Table 1 left unclassified by Jackson & Rawlings (1997) finds their ground-based spectra likewise non-thermally dominated. The spectra of galaxies classified as E type, in some cases (e.g., 3C 348), but not all show optical spectra dominated by host galaxy starlight (Tadhunter et al. 1993). To be conservative, we have listed m_1 mags as a limit on the nuclear brightness of galaxies of type E in Table 3. This relative inaccuracy in our nuclear magnitude estimates does not affect our final results.

4. Clustering Analysis

This work utilizes B_{gg} , the amplitude of the galaxy-galaxy spatial covariance function, as a quantification of the richness of the clustering environment around a given object. Given a cosmology, an assumed evolution of the galaxy luminosity function and measured mean background galaxy counts, this parameter reflects the galaxy overdensity around a given object, correcting for the expected spatial and luminosity distributions of field galaxies and of the associated cluster galaxies at the redshift of the object.

This parameter is described in detail in Longair & Seldner (1979) and the specific technique used in obtaining the actual values of B_{gg} is described in Yee & Green (1987) and EYG. Briefly, the technique is as follows. All galaxies within 0.5 Mpc of the radio source brighter than some

magnitude are counted. Then the expected number of background galaxies in that area down to the same magnitude is subtracted. The number of excess galaxies is normalized to an evolved galaxy luminosity function at the redshift of the object and then converted to B_{gg} assuming a form for the spatial distribution of galaxies.

As explained in EYG, the 0.5 Mpc counting radius is chosen to provide good contrast between cluster and foreground/background galaxies and to minimize the effects of the variation of the actual spatial distribution of the cluster galaxies from the assumed form. The magnitude limit for galaxy counting is determined for each field individually and is taken to be the brighter of the “completeness” magnitude, m_{comp} , or $M_r^* + 2.5$. Background galaxy counts are those of Yee et al. (1996,1998). The evolving galaxy luminosity function used to normalize the excess galaxies includes moderate galaxy evolution of $M_*(z) \sim z$ (EYG). Finally, the distribution of the excess galaxies is assumed to be the standard cluster galaxy power law ($r^{-\gamma}$ where $\gamma = 1.77$). This originates from the angular distribution of Seldner & Peebles (1978) and was used by both Yee & Green (1987) and EYG. Yee & Green (1987) show this assumption is consistent with their results.

It should be noted that although B_{gg} is a measure of the excess galaxies around a given object, a large value of B_{gg} does not prove absolutely that there is a cluster around any individual object. The excess galaxies could be due to an anomalous overdensity of foreground and/or background galaxies in that region of the sky. Although galaxy colors can be used as an indication of the redshift of the excess galaxies, only spectroscopic observations can completely confirm cluster membership. For those who are more familiar with the cluster richness classification of Abell (1958): B_{gg} values of 600 ± 200 , 1000 ± 200 , 1400 ± 200 , and 1800 ± 200 Mpc^{1.77} are comparable to Abell richness classes 0, 1, 2, and 3, respectively (Yee & López-Cruz 1999). EYG chose $B_{gg} = 500$ Mpc^{1.77} to define the boundary between rich and poor environments because, at the time, it was thought to be the division between Abell richness classes 0 and 1 (Prestage & Peacock 1988, 1989). We adopt this boundary for consistency with the earlier work and show below that this choice does not affect our results significantly.

The total uncertainty in B_{gg} is given by $\Delta B_{gg}/B_{gg} = (N_{net} + 1.3^2 N_b)^{1/2}/N_{net}$ (Yee & López-Cruz 1999) where N_b is the expected number of background galaxy counts and $N_{net} = N_{total} - N_b$ is the number of excess galaxy counts. This uncertainty is obtained by adding two terms in quadrature. The first term, $(N_{net})^{1/2}/N_{net}$, is the internal statistical error in sampling the associated cluster galaxy luminosity function using a finite number of galaxies. The second term, $1.3(N_b)^{1/2}/N_{net}$ (EYG), is the error due to the uncertainty in the background galaxy counts. The factor of 1.3 is an empirical value that accounts for the clustering of the background galaxies which causes the error in the background galaxy counts to deviate from a Poisson error. This factor is discussed in detail in Yee et al. (1986). The error in B_{gg} is often quite a substantial fraction of the B_{gg} value due to the small number of “excess” galaxies relative to the expected number of field galaxies. Two of the quasar fields we observed (3C 323.1 and 3C 351) were also observed by YE93. A comparison of our B_{gg} values with theirs shows differences within the uncertainties that are easily attributable to differences in the limiting magnitudes.

4.1. Incorporation of Other Clustering Data

We have measured B_{gg} for 39 of the 79 fields in our sample. However, measures of the excess galaxies surrounding many additional objects exist in the literature in one form or another and have been incorporated into this study. Table 5 provides a comparison between our method of measuring B_{gg} and the other methods of measuring the number of excess galaxies. The differences between methods and the conversions to our B_{gg} values are discussed below for each method listed in Table 5.

4.1.1. *Yee & Ellingson (1993)*

Nuclear magnitudes and B_{gg} values for 63 quasars (8 of which are 3CR sources) with $0.15 < z < 0.7$ were taken directly from YE93, which includes the samples used in EYG. These B_{gg} values were obtained in a manner almost identical to our own. Some of their values (those taken from YG and Yee & Green (1984)) were calculated using $q_0 = 0.5$ with a slightly different luminosity function (that of Sebok (1986) rather than the luminosity function of King & Ellis (1985) that we used; see YG) and with slightly different background counts, but these differences are minor. We have thus taken their values without any correction. As mentioned above, comparisons of B_{gg} values for objects in common agree to within the uncertainties.

4.1.2. *Zirbel (1997)*

Zirbel (1997) observed a sample of radio galaxies (of which 27 are in the 3CR sample in our redshift range) and quantified the galaxy environment using $N_{0.5}^{-19}$ (or “richness”): the number of excess galaxies brighter than $M_V = -19$ within a 0.5 Mpc radius of the object. The main differences between this method and our method are that the images are in V rather than Gunn r , the limiting magnitude is fixed for all fields, and galaxies that are -0.6 mag bluer or 0.2 mag redder than an elliptical galaxy of the same absolute magnitude are excluded from the excess galaxy counts. Since these galaxies are red, faint galaxies that would be detected in Gunn r may not be detected in V. The fixed limiting magnitude of $M_V = -19$ means that we tend to count galaxies down to fainter magnitudes, especially at lower redshifts ($z < 0.3$), but this should be accounted for in the normalization. The effect of excluding galaxies with anomalous colors is to reduce the number of excess galaxies. So, in general, we expect the number of excess galaxies measured by Zirbel (1997) to be less than ours. Since B_{gg} is directly proportional to the number of excess galaxies, we expect the $N_{0.5}^{-19}$ values of Zirbel (1997) to be converted to our B_{gg} values by a multiplicative constant. Since a correction for the luminosity evolution of the galaxies is made by Zirbel (1997) (see Allington-Smith et al. (1993) for details), this multiplicative constant is expected to be the same for all fields regardless of redshift. However, the differences between the two methods discussed above will cause a slight variation in this multiplicative constant from field to field and

so there will be some scatter around the actual conversion value.

In order to determine this conversion constant, a weighted least squares linear fit of Zirbel’s “richness” values to our B_{gg} values was performed using 13 objects for which we both had data. The fit was forced through the point (0,0) because zero excess galaxies should give $B_{gg} = 0$. The resulting conversion is $B_{gg} = 38N_{0.5}^{-19}$. The fit and the data points with their error bars are shown in Figure 1. The 1σ error bars for all but 3 of the points overlap the fit and the farthest of these 3 points (3C 348) lies within 2σ of the fit.

4.1.3. *Yates, Miller & Peacock (1989; YMP)*

This work includes data from 14 3CR radio galaxies in our redshift range. The B_{gg} values are the same quantity that we calculate. However, their values are not directly comparable to ours due to differences in methodology and so a conversion is still required. While their model 2b is the closest to our work ($q_0 = 0$, a King & Ellis (1985) luminosity function, YG normalization and evolution), they do not distinguish between stars and galaxies when counting objects, the area over which they count objects varies from field to field and their computation of the completeness magnitude is different from ours. Although the inclusion of stars to their number counts sounds like a crucial difference, it should be accounted for by their “local” (5' to 10' offset) measurement of background objects (stars and galaxies). This assumes that there are no large differences in the stellar number density between an object field and its offset frame. However, not directly eliminating the stars from the analysis increases the random uncertainty in B_{gg} . Yates, Miller & Peacock (1989) also take their completeness magnitude to be at the peak of their galaxy number distribution whereas we take it to be where the galaxy number distribution begins to drop below the expected linear form. This will cause Yates, Miller & Peacock (1989) to overestimate their completeness magnitude, giving them lower counts and a lower value of B_{gg} than ours for the same completeness magnitude. However, the non-uniform variation of both our completeness magnitude and that of Yates, Miller & Peacock (1989) from field to field prevents this from appearing as a systematic difference in the objects we both observed.

We can attempt to model the effects of the differences between our method and that of Yates, Miller & Peacock (1989) as an additive offset between the two B_{gg} values. Thus, we look for a conversion of the form: $\{\text{our } B_{gg}\} = \{\text{YMP } B_{gg}\} + \text{constant}$. Note, however, that the variation of the differences in the two methods from field to field may cause this offset to vary. An average offset of 70 was determined from 5 of the 7 objects for which we both had data. The remaining two objects (3C 346 and 3C 348; the uppermost points of Figure 2) were not used in the determination of this offset because they both had extremely small counting areas when compared to ours (smaller by a factor ~ 3) and so represented extreme rather than typical differences. A comparison of this “average offset” conversion to a weighted least squares linear fit to the same 5 points is shown in Figure 2. The offset conversion is given by the solid line. The two lines agree to within their error bars ($y = x + 70 \pm 147$ vs. $y = 0.91 \pm 0.54 \times x + 105 \pm 73$) and when the size of the error bars of the

points is considered, the difference between the two fits is quite small. Only 3C 348 is noticeably offset from the fit and it is still well within 2σ .

4.1.4. Hill & Lilly (1991; HL)

Hill & Lilly (1991) observed a sample of radio galaxies at $z \sim 0.5$, 13 of which are included in this study. Their measurement of $N_{0.5}$ is derived from the number of excess galaxies within a 0.5 Mpc radius of the object within the magnitude range m_1 to $m_1 + 3$ where m_1 is the magnitude of the object. We note that this method does include a built-in correction for galaxy evolution and k-corrections, as long as the radio galaxies can be considered typical of cluster galaxies. This quantity is computed using $q_0 = 0.5$. Another listed quantity, $N_{0.5}^M$, is the same as $N_{0.5}$ except that the mean m_R - z relation for the object is used as m_1 rather than the magnitude of the object itself. A third tabulated quantity, $N_{0.5}^0$, is the same as $N_{0.5}$ except that $q_0 = 0$ was used in the calculation. Although this third quantity is a closer match to our value of q_0 , the second quantity is more consistent with our method of determining the limiting magnitude. Using the $N_{0.5}^M$ values, the differences between our method and that of Hill & Lilly (1991) are the different value of q_0 , the slightly different optical waveband, variations in the limiting magnitude from field to field, and the fact that they do not distinguish between stars and galaxies. The effects of varying q_0 are negligible compared with the uncertainties. The difference in optical waveband is small (R vs. Gunn r), and should not systematically affect the results as long as both field and background counts are observed in the same band. Varying the limiting magnitude should have no systematic effect on the results, but can produce statistical variations in different measurements for individual objects, depending on how deep the luminosity function is sampled. Finally, as with Yates, Miller & Peacock (1989) above, the local measurement of background objects should account for stars not being removed but the potential for much larger errors is increased.

As with the $N_{0.5}^{-19}$ values of Zirbel (1997), we expect the conversion of the Hill & Lilly (1991) $N_{0.5}^M$ values to our B_{gg} to be in the form of a multiplicative constant. Hill & Lilly (1991) account for luminosity evolution by using the radio galaxy magnitude to define an epoch-invariant point on the luminosity function and then referencing the magnitudes of all galaxies in the counting region of the field to that of the radio galaxy. They note that this method yields values that are $\sim 20\%$ higher than those from the method that we have adopted. Thus, the conversion constant might actually be a function of redshift. However, the objects in Hill & Lilly (1991) that are in our sample have a relatively narrow redshift range ($z = 0.367$ to $z = 0.5524$) and so we assume a single multiplicative constant for the conversion of all values regardless of redshift. Although we had no data in common with Hill & Lilly (1991), we had 1 B_{gg} value from YE93 and 10 converted B_{gg} values from Zirbel (1997) that overlapped with the Hill & Lilly (1991) data. A weighted least squares linear fit forced through the point (0,0) was performed using all 11 of these objects, resulting in the conversion $B_{gg} = 33N_{0.5}^M$. The fit and the data points with their error bars are shown in Figure 3. This conversion lies between the empirical conversion ($B_{gg} = 30N_{0.5}$) and the theoretical conversion ($B_{gg} = 34N_{0.5}$)

given in Hill & Lilly (1991). Also, the somewhat lower conversion factor of the Hill & Lilly (1991) $N_{0.5}^M$ values as compared to that of the Zirbel (1997) $N_{0.5}^{-19}$ values (33 vs. 38) is consistent with the relationship between these values quoted in Allington-Smith et al. (1993), to within the error bars.

4.2. Summary of All Clustering Data

A compilation of the B_{gg} values from all the methods discussed above is given in Table 6. Discrepancies and uncertainties are discussed in the notes following the table and a key to the references is given after the notes. Errors for our values were discussed at the beginning of Section 4. Errors for the YE93 values were taken directly from the literature. Errors for the converted B_{gg} values (those from Zirbel (1997), Hill & Lilly (1991) and Yates, Miller & Peacock (1989)) were computed by converting the original 1σ values to B_{gg} values and using this spread in the converted B_{gg} value as the error.

“Adopted” B_{gg} values are listed in Table 7. Sixty five of the 79 objects in this complete 3CR sample have B_{gg} values. Because the absence of B_{gg} data is due entirely to the absence of photometric images and because the order in which objects were observed was random, there is no bias introduced due to this incompleteness in the B_{gg} data. In the absence of our own value, the value from YE93 was used in Table 7, if available; otherwise converted B_{gg} values were used. Since we had no data in common with Hill & Lilly (1991), this conversion is indirect and so the values of Zirbel (1997) were judged to generally be the most reliable of the converted values, followed by those of Hill & Lilly (1991) and then those of Yates, Miller & Peacock (1989). Different converted values for the same field that agreed to within their errors were averaged together. Two objects (3C 275 and 3C 435A) have a range of B_{gg} values listed in Table 7 because other studies yielded highly discrepant values and, in the absence of other data, it is unclear which of the values is more reliable in these specific cases.

The distribution of the B_{gg} values listed in Table 7 is shown in Figure 4. The two objects (3C 275 and 3C 435A) with a range of B_{gg} values listed in Table 7 are omitted from Figure 4 and from all further analysis and discussions. Table 7 contains 17 sources with $B_{gg} > 500 \text{ Mpc}^{1.77}$. The richness of all 17 of these fields has been previously noted in one form or another in the literature. Most notably, 3C 28 has the richest environment (excluding the upper limit on the range for 3C 435A) and is a known Abell cluster (Abell 115) and a known X-ray cluster (McCarthy et al. 1995 and references therein). In addition to the references listed in Tables 6 and 7, information on the fields surrounding the remaining sources with $B_{gg} > 500 \text{ Mpc}^{1.77}$ can be found in Wyndham (1966), Kristian, Sandage & Karem (1974, 1978), Hintzen & Stocke (1986), Ellingson et al. (1991b), Spinrad et al. (1991) and references therein, Ellingson et al. (1994), McCarthy et al. (1995), Hall et al. (1995), Rector, Stocke & Ellingson (1997), Hes et al. (1996) and Gizani & Leahy (1999).

5. Results

5.1. Radio Galaxy Environments vs. Quasar Environments

The environments of the two samples must be compared as a function of redshift because EYG have shown that quasar environments vary dramatically with redshift. Figure 5 shows the sample plotted both as a function of redshift and absolute nuclear B magnitude. Sources located in rich environments ($B_{gg} > 500 \text{ Mpc}^{1.77}$) are denoted by filled symbols while those in poor environments ($B_{gg} \leq 500 \text{ Mpc}^{1.77}$) are marked with open symbols. The absolute nuclear B magnitude is in general agreement with the AGN classification; i.e., all quasars have $M_B < -22.5$ while all but 4 of the radio and N-galaxies have $M_B > -22.5$. For consistency, the 4 galaxies with $M_B < -22.5$ are reclassified as quasars for the environment comparisons discussed below (this has no significant effect on the results).

Note the gap in magnitude between the quasars and most of the radio galaxies in Figure 5. It is unclear whether this gap is real or due to possible systematic differences in the way the absolute nuclear B magnitude was calculated for quasars and radio galaxies. Quasars were assumed to have a negligible host galaxy contribution and so a total magnitude was used for the nuclear magnitude. For radio galaxies, a magnitude in the inner 1-2 kpc was used to estimate the nuclear magnitude. The systematic effect of including the host galaxy contribution in the quasar nuclear magnitudes can be estimated using a “typical” AGN host galaxy magnitude of $M_{host_B} = -22$. (estimated from the radio galaxy data in Table 3). Removing such a contribution makes an $M_B = -23$ quasar nuclear magnitude dimmer by 0.6 mag. Thus, the net effect would be to spread out the lower envelope of the quasar nuclear magnitude distribution, but this is insufficient to close the gap in Figure 5 entirely. So it seems possible that some systematic differences in magnitudes could be present. Still, this systematic is not large enough to cause a significant overlap of quasar and radio galaxy absolute nuclear B magnitudes (i.e., few objects would be misclassified).

Also plotted in Figure 5 is a very low z ($z < 0.1$) sample of radio galaxies, taken from YE93, which contains a mixture of FR1 and FR2 type sources (all those at $z < 0.1$ with $B_{gg} > 500 \text{ Mpc}^{1.77}$ are FR1s). Although it has been included on this plot, this sample is NOT included in any comparison between quasar and radio galaxy properties because there are no quasars at this low redshift. Originally, the case for an evolutionary fading model for quasars was made by EYG on the basis of their quasar sample at $z > 0.3$ and this very low z ($z < 0.1$) sample of radio galaxies. The data from the present work fill the ~ 4 Gyr gap between these two samples.

An inspection of just the quasars in Figure 5 shows that there are a substantial number of quasars found in rich environments at $0.4 < z < 0.65$ but there are none found in rich environments at $z < 0.4$. This dramatic result is presented and discussed in EYG and YE93 and is the basis for their evolutionary hypothesis. We choose the $0.15 < z < 0.4$ redshift range in which to compare radio galaxy and quasar environments because of the striking absence of quasars in rich environments at these redshifts. The orientation angle hypothesis of Barthel (1989) predicts that

the percentage of quasars found in rich environments at $0.15 < z < 0.4$ should be the same as the percentage of radio galaxies found in rich environments over that same redshift range. However, a Kolmogorov-Smirnov test yields only a 3% chance that the two distributions of B_{gg} values were drawn from the same parent population (Figure 6). On this basis the orientation angle hypothesis of Barthel (1989) is rejected at the 97% (2.2σ) confidence level.

Since N-galaxies do have a strong point source component, it is possible that N-galaxies are actually quasars with either a slightly lower luminosity AGN or a slightly brighter host galaxy. If the above analysis is redone with *all* N-galaxies grouped together with the quasars (rather than grouping those with $M_B > -22.5$ with the radio galaxies), the difference in the environments of the radio galaxies and quasars at $0.15 < z < 0.4$ becomes even larger: a KS test gives only a 0.4% chance, or a rejection at the 3σ level, that the two distributions come from the same parent population.

Because the AGN nuclear magnitudes are drawn from a continuous luminosity function with a somewhat unclear observational magnitude limit, we follow YE93 and quantify the relative evolution of rich and poor environments by building a model of the brightest AGN one would expect to see, as a function of redshift. We use the two-power-law model of the quasar luminosity function from Boyle et al. (1988), with evolution in the characteristic quasar luminosity parametrized as $L^*(z) = L_0(1+z)^{\kappa_L}$. This luminosity function is used along with the relation for cosmological volume as a function of redshift, to produce a family of curves describing the brightest AGN one would see at any given redshift, for various values of the rate of evolution, κ_L . The curves are normalized empirically to $z \sim 0.6$, where the brightest radio-loud quasars observed in the 3CR sample are often found in rich environments.

In agreement with YE93, we find the “standard model” ($\kappa_L = 3.7$; solid line) to be a good fit to the upper envelope of all the data in Figure 5. This model is based on the well-determined parameters for optically-selected quasars, and hence describes the general population of very luminous AGN, which here are mostly located in poor environments. The model corresponding to $\kappa_L = 19$ (dash-dot line) was found to be the best match for the upper envelope of the data when only the sources in rich environments in Figure 5 (i.e., only the filled symbols) were used.

An upper limit on the e-folding time (τ) for the fading of quasars can be obtained by assuming an exponential form for the luminosity evolution, $L^*(z) = L_0 e^{t/\tau}$. For sources in rich ($B_{gg} > 500 \text{ Mpc}^{1.77}$) environments (i.e., $\kappa_L = 19$) at $z = 0.4$ (the middle of our redshift range), the resulting e-folding time for quasars is 0.9 Gyr for $H_0 = 50, q_0 = 0$ (0.6 Gyr for $H_0 = 75, q_0 = 0$). Comparing the κ_L values of these fits to the upper envelope of the sources in poor ($\kappa_L = 3.7$) and rich ($\kappa_L = 19$) environments, it appears that sources in rich environments evolve ~ 5 times faster than those in poor environments. Changing the B_{gg} value that defines a rich environment from 500 to 400 or 600 $\text{Mpc}^{1.77}$ has little effect on these results. The upper envelope of the sources with $B_{gg} > 400 \text{ Mpc}^{1.77}$ is well fit by the model corresponding to $\kappa_L = 16$ while that of the sources with $B_{gg} > 600 \text{ Mpc}^{1.77}$ is well fit by a $\kappa_L = 24$ curve. The e-folding times associated with these values of κ_L

vary by only $\sim 20\%$ (a 19% increase in τ for $\kappa_L = 16$ and a 21% decrease in τ for $\kappa_L = 24$) from those corresponding to the $\kappa_L = 19$ curve. While changing the definition of a rich environment to $B_{gg} > 700 \text{ Mpc}^{1.77}$ still has little effect on the results (the $\kappa_L = 24$ model is still a good fit to this upper envelope), dropping the limit to $B_{gg} > 300 \text{ Mpc}^{1.77}$ has a drastic effect. In this case, the standard envelope model ($\kappa_L = 3.7$) is a good fit and the e-folding times increase by more than a factor of 5.

Although the evidence presented above makes it very unlikely that the orientation angle hypothesis of Barthel (1989) is the primary means of relating quasars and radio galaxies, it is possible that *some* quasars are radio galaxies with their jet oriented close to our line of sight (within $\sim 45^\circ$). Thus, Barthel's hypothesis may be valid for individual objects but it is almost certainly not valid for the AGN population as a whole. Also, we cannot rule out that quasars and radio galaxies are related to one another by some combination of both evolution and orientation.

5.2. Correlations Between Environment and Other AGN Properties

Since the 3CR sample is flux-limited, the radio power and redshift are highly correlated ($r = 0.65$ at a confidence level $> 99.9\%$). Thus, there is the possibility that the distribution of the objects in rich environments seen in Figure 5 is actually due to a correlation between radio power and environment at a given redshift combined with the radio power-redshift correlation of the 3CR sample. Yates, Miller & Peacock (1989) do find a slight correlation between radio power and environment in their study of radio galaxies, as do Wold et al. (2000). Hill & Lilly (1991), whose study of radio galaxies is well-suited to answer this question because of its large range of radio powers and its relatively narrow redshift range, find no evidence of a correlation between radio power and environment at $z \sim 0.5$.

In Figure 7, the total radio power at 178 MHz of all the 3CR objects used in this study (including the radio galaxies with $z < 0.1$ taken from YE93 which are not part of the present sample) are plotted versus redshift with filled symbols indicating objects with $B_{gg} > 500 \text{ Mpc}^{1.77}$. The symbols have the same meaning as in Figure 5 and quasars with unknown environments are marked with an “X”. A visual inspection of Figure 7 shows that, with a few exceptions, for each object in a rich environment there are objects at a similar redshift in a poor environment with equal or greater radio power (i.e., the objects in rich environments, in general, are not the most powerful radio sources at a given redshift). Ignoring the objects with $z < 0.1$, a correlation analysis using the remaining 3CR objects (i.e., those in the sample of this work) yields a correlation coefficient between radio power and environment of $r = 0.27$ at a confidence level of $\sim 97\%$. Thus, there does appear to be a slight correlation between radio power and environment for the objects in the present sample but not as strong a correlation as would be required to create the apparent evolutionary effect seen in Figure 5.

Figure 8 shows the complete sample, including the quasars which are not 3CR sources. While

a number of these objects lie at somewhat lower radio powers than the radio galaxies at similar redshifts, their powers are still well above many radio galaxies which are located in clusters. The lack of clusters in this sample is thus difficult to explain in a unified model. We note that about 10% of the quasar sample may be core dominated (Rector, Stocke & Ellingson 1997, Hutchings et al. 1998), indicating that their total radio powers may be overestimates of their lobe power. However, these objects are found in both rich and poor environments, suggesting that this does not strongly affect the comparison of radio galaxies and quasars.

Additionally, there is no significant correlation between total M_r (and thus host galaxy M_r) and B_{gg} , although virtually all of these FR2 host galaxies are much more luminous than M^* . Specifically, eight of the nine FR2s with M_r determined and $B_{gg} \geq 500 \text{ Mpc}^{1.77}$ have absolute host luminosities 1-2 mags brighter than M^* (3CR 435.0A is the lone exception with a poorly determined magnitude 0.5 mags less luminous than M^*). These values are typical of poor cluster brightest cluster galaxies (Hoessel, Gunn & Thuan 1980; Wurtz et al. 1997), and, as found by other studies (Lilly & Prestage 1987; Allington-Smith et al. 1993), the radio galaxies are the brightest members of their groups and poor clusters.

Finally, we briefly examined the relationship between the environment and the optical class (column 9 of Table 1) of each source. The distribution of B_{gg} values was found to be similar for all optical classes and no significant difference in the percentage of rich environments ($B_{gg} > 500 \text{ Mpc}^{1.77}$) for each optical class was found. So, based on the correlation analyses discussed above, the behavior illustrated in Figure 5 appears to be genuine and not due to secondary and/or multiple correlations of the various other AGN parameters.

6. Conclusion

6.1. Summary of the Results

The results of this work are summarized below:

1. A comparison of the environments of 51 radio galaxies and 67 quasars in the redshift range $0.15 < z < 0.65$ clearly shows that while quasars are found in rich environments ($B_{gg} > 500 \text{ Mpc}^{1.77}$; i.e., Abell richness class 0 and above) only at $z > 0.4$ (EYG), radio galaxies are found in rich environments over the entire redshift range with the percentage of radio galaxies in rich environments at $0.15 < z < 0.4$ (20%) being comparable to that of radio galaxies in rich environments at $0.4 < z < 0.65$ (28%) and quasars in rich environments at $0.4 < z < 0.65$ (36%). A K-S test gives only a 3% chance that the B_{gg} distributions of the radio galaxies and quasars at $0.15 < z < 0.4$ come from the same parent population. On this basis, the orientation angle hypothesis of Barthel (1989) is rejected at the 97% (2.2σ) confidence level as the primary means of relating quasars and radio galaxies. If all N-galaxies are grouped with the quasars, the hypothesis of Barthel (1989) is rejected at the 99.6% (3σ) confidence level. However, a combination of Barthel's

orientation hypothesis and EYG’s evolutionary hypothesis cannot be ruled out.

2. Applying the evolutionary model (pure luminosity evolution; i.e., no number density evolution) described in YE93, we find that the “standard envelope model” ($\kappa_L = 3.7$) is a good fit to the upper envelope of the sources in poor environments while a model corresponding to $\kappa_L = 19$ matches the upper envelope of the sources in rich ($B_{gg} > 500 \text{ Mpc}^{1.77}$) environments. A comparison of these two values of κ_L implies that sources in rich environments evolve ~ 5 times faster than those in poor environments. Converting κ_L to an e-folding time (τ), the maximum e-folding time for quasars in rich ($B_{gg} > 500 \text{ Mpc}^{1.77}$) galaxy environments is $\tau \sim 0.9 \text{ Gyr}$ for $H_0 = 50, q_0 = 0$ ($\tau \sim 0.6 \text{ Gyr}$ for $H_0 = 75, q_0 = 0$). All these results are in excellent agreement with YE93 and are not strongly dependent upon the exact choice of B_{gg} used to define a rich environment.

3. It is unlikely that the redshift relationship between the radio galaxies in rich environments and the quasars in rich environments seen in Figure 5 is due to a correlation between radio power and environment coupled with the redshift-radio power correlation of the flux-limited 3CR sample. Nor do any other secondary or multiple correlations appear to be responsible.

6.2. A Compatible Hypothesis

In this Section we describe a compatible hypothesis for the results presented here. This hypothesis links the observed evolution of AGN activity in clusters with the decline of individual sources in response to evolution in their cluster environment. While this may not be the only physical mechanism that could account for these results (e.g., systematic changes in jet opening angle with time for AGN in clusters is another possibility), the scenario we propose is simple and consistent with both theoretical ideas about the triggering of quasars and observational constraints on the evolution of the cluster gravitational potential well from X-ray observations. The ideas presented below also are most easily understood in a model by which a single cluster AGN undergoes secular evolution in power, instead of a statistical fading of cluster AGN as a population. While either possibility is consistent with current data, we note that cD galaxies in rich clusters in the current epoch are luminous radio emitters (i.e., typically $\log P_{rad} \geq 25 \text{ W Hz}^{-1}$) 35-40% of the time. So in the case of the cD galaxies, like those in which the quasars and radio galaxies in this study are located, a large fraction of the full population of such objects is radio-loud at any one time, unless the current epoch statistics are very anomalous. Since several lines of argument suggest that single radio source lifetimes are 10^{7-8} yrs, every cD galaxy must have “turned on” several times in the last few Gyrs to account for the current epoch statistics. Therefore, particularly for the cD galaxies, a recurrent outburst hypothesis is particularly attractive, and so we will assume that this idea is correct in the discussion below.

The triggering of quasars is believed to be caused by galaxy-galaxy interactions and mergers (e.g., Roos 1981; Barnes & Hernquist 1992; Wilson & Colbert 1995). However, the rate and relative velocities of these interactions and mergers change as the clustering environment around the

quasar evolves. In the early stages of cluster formation, the duration of galaxy-galaxy interactions tends to be longer because the cluster potential well is still shallow and the galaxies have not yet reached their full orbital speed. In this stage of cluster evolution, mergers are still efficient at destroying disk structures and transferring gas (e.g., Mihos 1995). However, as a cluster virializes and begins to come into dynamical equilibrium, the orbital speeds of the galaxies increase and the galaxy orbits stabilize. Galaxy-galaxy mergers and interactions become less frequent and are of shorter duration, making them less effective at triggering AGN activity (Aarseth & Fall 1980; Roos 1981; Wilson & Colbert 1995).

Several authors (e.g., Blandford & Znajek 1977; Begelman, Blandford & Rees 1980; Wilson & Colbert 1995) have suggested that, unlike radio-quiet AGN, radio-loud AGN are powered by the spin energy extracted from very rapidly spinning supermassive black holes (SMBHs). Rapidly spinning SMBHs can be formed most easily from the capture and subsequent orbital evolution of a SMBH binary system (on a timescale of 10^8 yrs after the binary pair is formed; but see Begelman, Blandford & Rees (1980) who advocate much longer timescales). Under certain circumstances, merging disk galaxies can provide non-rotating SMBHs from their nuclei (Wilson & Colbert 1995) and the eventual merger of the SMBH pair forms the very rapidly spinning SMBH, whose spin energy is extracted by the Blandford-Znajek mechanism to create the radio jets and other radio-loud quasar manifestations. As the cluster virializes, the absence of suitably slow encounters prevents the formation of new SMBH binaries as well as the injection of mass into the region of the SMBH. Thus, the existing SMBH can only spin down as it releases energy, creating lower power outbursts over time; i.e., a luminous quasar at $z \sim 0.5$ fades to become an FR2 radio galaxy then an FR1 radio galaxy. In this picture, the fading timescale of 0.9 Gyrs found by this work is the spin down time for the SMBH.

Alternately, the quasar is starved of fuel as the cluster virializes. The nuclear engine of the quasar (i.e., the AGN) is believed to be fueled by gas from either the quasar host galaxy or from an interacting companion galaxy (Roos 1981, 1985; De Robertis 1985). In the early stages of cluster formation, galaxies are believed to contain an abundance of gas and so fuel for the AGN is plentiful. However, as a cluster develops, an intracluster medium (ICM) begins to form due to the combined remnants of galaxy-galaxy interactions and mergers (e.g., tidal tails). As the ICM becomes dense ($> 10^{-4} \text{ cm}^{-3}$), it will begin to strip or “sweep” gas out of the galaxies moving through it (Stocke & Perrenod 1981), making itself more dense and even more effective at “sweeping” gas (Gisler 1976). As the gas sweeping ability of the ICM increases, potential fuel for the AGN is more easily stripped from cluster galaxies moving through the medium and heated to X-ray emitting temperatures. This positive feedback loop may eventually starve the AGN (by decreasing the gas reservoir in both the AGN host galaxy and the interacting companion galaxies) causing it to dim.

In this scenario, therefore, the evolution of the fraction of AGN seen in clusters probes the systematic evolution of the physical conditions within the cluster environment. Because of their sensitivity to local conditions, the most optically luminous AGN mark primarily poor groups *or* those richer systems which are in the early stages of virilization. Thus, clusters of a given richness

will no longer harbor quasars past a certain epoch. For clusters having a richness of $B_{gg} \sim 500$ Mpc^{1.77}, this epoch is $z \sim 0.4$ (EYG). This quasar dimming will occur at an earlier epoch for even richer environments than those discovered here (i.e., Abell richness class 2 and higher) while for poorer environments it will occur closer to the present time. That is, to our knowledge, no quasar or luminous radio galaxy (i.e., FR2) has been discovered in an *extremely* rich cluster ($B_{gg} > 1500$ Mpc^{1.77}) at $z < 0.65$. The scenario described here suggests that this absence occurs because the ICM in extremely rich clusters is already too dense and quasars therein have been “starved” at earlier epochs. Thus, by $z \sim 0.6$ these AGN have faded through luminous FR2 radio galaxies to become low power FR1 radio galaxies. The study of radio sources in the richest cluster environments ($B_{gg} > 1500$ Mpc^{1.77}) at $z = 0.3 - 0.8$ by Stocke et al. (1999) supports this suggestion, finding only FR1 type sources in these clusters.

The maximum evolutionary e-folding time of ~ 0.9 Gyr is a factor of several shorter than the virialization timescale for the entire cluster; however, quasar evolution is more likely to be affected by the conditions in the cluster core region, rather than the 1 Mpc scale environment. Thus, even if cluster virialization triggers the fading of these quasars, the fading itself occurs too rapidly to be “tracking” the subsequent cluster evolution. However, evolution of the cluster core could “track” quasar fading. Assuming a cluster core radius of 0.1 - 0.25 Mpc (based on the extent of X-ray emission from clusters; Henry et al. 1992) and 5 crossing times for virialization, the virialization time of a cluster core would be $\sim 1 - 2.5$ Gyr which is more comparable to the quasar fading time we find above. Therefore, while cluster virialization initially “starves” the quasar by one or both of the mechanisms above, the actual fading timescale must be due to some internal AGN clock, not to any timescale in the larger environment of the AGN, all of which are too long.

6.3. Further Tests of This Hypothesis

Additional studies can test some of the ideas proposed in this work. Based on the scenario presented above, clusters of richness $B_{gg} \gtrsim 500$ Mpc^{1.77} at $z > 0.4$ hosting AGN would be expected to have lower velocity dispersions and higher fractions of blue, star-forming galaxies than clusters of similar richness at $z < 0.4$ (e.g., Ellingson et al. 1994). The link between ICM and AGN activity would suggest that AGN-hosting clusters of richness $B_{gg} \gtrsim 500$ Mpc^{1.77} at $z < 0.4$ have a denser ICM than clusters of similar richness at $z > 0.4$; Hall et al. (1995) show that extended X-ray luminosities around quasars fall in the lower range of what is expected from clusters of similar richness. A more conclusive test of this hypothesis could be performed using sensitive, high resolution X-ray images such as those from ACIS aboard Chandra to search for direct detections of a dense, hot ICM surrounding both the quasars and radio galaxies at $z < 0.4$. An indirect investigation of the ICM surrounding the sources studied here using the extended radio morphology of these sources is presented in Paper 2; the results support this hypothesis and suggest that a dense ICM can affect extended radio structure and may even cause FR2 type radio sources to evolve into FR1-like structures at $z < 0.4$.

We wish to thank KPNO for telescope time and support given to us for this project. M.H. acknowledges the support of a NASA Graduate Student Research Program Fellowship NGT - 51291 and the travel support of NOAO to conduct these thesis observations. EE would like to acknowledge NSF grant AST-9617145. H.K.C. Yee is thanked for the use of his PPP program and for numerous helpful discussions. G. Hill is also thanked for his cooperation. This research has made use of the NASA/IPAC Extragalactic Database (NED) which is operated by the Jet Propulsion Laboratory, California Institute of Technology, under contract with NASA.

REFERENCES

Aarseth, S.J., & Fall, S.M. 1980, *ApJ*, 236, 43

Abell, G.O. 1958, *ApJS*, 3, 211

Allington-Smith, J.R., Ellis, R.S., Zirbel, E.L., & Oemler, A. 1993, *ApJ*, 404, 521

Baars, J. W. M., Genzel, R., Pauliny-Toth, I. I. K., & Witzel, A. 1977, *A&A*, 61, 99

Barnes, J.E., & Hernquist, L. 1992, *ARA&A*, 30, 705

Barthel, P.D. 1989, *ApJ*, 336, 606

Begelman, M.C., Blandford, R.D., & Rees, M. J., 1980, *Nature*, 287, 307

Bennett, A.S. 1962, *MmRAS*, 68, 163

Blandford, R.D., & Znajek, R.L. 1977 *MNRAS*, 179, 433

Boyle, B.J., Shanks, T., & Peterson, B.A. 1988, *MNRAS*, 235, 935

Burstein, D., & Heiles, C. 1982, *AJ*, 87, 1165

Cardelli, J.A., Clayton, G.C., & Mathis, J. S. 1989, *ApJ*, 345, 245

de Koff, S., Baum, S.A., Sparks, W.B., Biretta, J., Golombek, D., Macchetto, F., McCarthy, P., & Miley, G.K. 1996, *ApJS*, 107, 621

De Robertis, M. 1985, *AJ*, 90, 998

de Vaucouleurs, G. 1948, *Ann. d'Astrophys.*, 11, 247

Ellingson, E., Yee, H.K.C., Bechtold, J., & Dobrzański, A. 1994, *AJ*, 107, 1219

Ellingson, E., Yee, H.K.C., & Green, R.F. 1991a, *ApJ*, 371, 49 (EYG)

Ellingson, E., Yee, H.K.C., & Green, R.F. 1991b, *ApJS*, 76, 455

Fanaroff, B.L., & Riley, J.M. 1974, *MNRAS*, 167, 31P

Feigelson, E.D., & Berg, C.J. 1983, *ApJ*, 269, 400

Fukugita, M., Shimasaku, K., & Ichikawa, T. 1995, *PASP*, 107, 945

Giovannini, G., Feretti, L., Gregorini, L., & Parma, P. 1988, *A&A*, 199, 73

Gisler, G.R. 1976, *A&A*, 51, 137

Gizani, N.A.B., & Leahy, J.P. 1999, *New Astronomy Reviews*, 43, 639

Gower, J. F. R., Scott, P. F., & Wills, D. 1967, MmRAS, 71, 49

Hall, P., Ellingson, E., & Green, R.F. 1995, AJ, 113, 1179

Hardcastle, M.J., Alexander, P., Pooley, G.G., & Riley, J.M. 1997, MNRAS, 288, 859

Harvanek, M., & Stocke, J.T., 2001, in prep. (Paper 2)

Heckman, T.M., Smith, E.P., Baum, S.A., van Breugel, W.J.M., Miley, G.K., Illingworth, G.D., Bothun, G.D., & Balick, B. 1986, ApJ, 311, 526

Hes, R., Barthel, P.D., & Fosbury, R.A.E. 1996, A&A, 313, 423

Hill, G.J., & Lilly, S.J. 1991, ApJ, 367, 1 (HL)

Hintzen, P., & Stocke, J. 1986, ApJ, 308, 540

Hoessel, J.G., Gunn, J.E., & Thuan, T.X. 1980, ApJ, 241, 486.

Hutchings, J., B. 1987, ApJ, 320, 122

Hutchings, J. B., Dewey, A., Chaytor, D., Ryneveld, S., Gower, A. C., & Ellingson, E. 1998, PASP, 110, 111

Jackson, N., & Rawlings, S. 1997, MNRAS, 286, 241

Kellermann, K. I., Pauliny-Toth, I. I. K., & Williams, P. J. S. 1969, ApJ, 157, 1

Kent, S.M. 1985, PASP, 97, 165

King, C.R., & Ellis, R.S. 1985, ApJ, 288, 456

Kristian, J., Sandage, A., & Katem, B. 1974, ApJ, 191, 43

Kristian, J., Sandage, A., & Katem, B. 1978, ApJ, 219, 803

Laing, R. A., & Peacock, J. A. 1980, MNRAS, 190, 903

Laing, R. A., Riley, J. M., & Longair, M. S. 1983, MNRAS, 204, 151

Lilly, S.J., & Prestage, R.M. 1987, MNRAS, 225, 531

Longair, M.S. 1985, in Radio Astronomy and the Physics of the Universe, ed. R. Fanti, G. Grueff, & G. Setti (Bologna: Istituto di Radioastronomia del CNR), 25

Longair, M.S., & Seldner, M. 1979, MNRAS, 189, 433

McCarthy, P.J., Spinrad, H., & van Breugel, W. 1995, ApJS, 99, 27

McCarthy, P.J., van Breugel, W., & Spinrad, H. 1989, AJ, 97, 36

Mihos, J.C. 1995, ApJ, 438, L75

Miley, G. 1980, ARA&A, 18, 165

NASA/IPAC Extragalactic Database 1997, Internet WWW page, at URL:
<<http://nedwww.ipac.caltech.edu/NED.html>>

Owen, F.N. 1986, in IAU Symp. 119, Quasars, ed. G. Swarup & V.K. Kapahi (Dordrecht: Reidel), 173

Pilkington, J. D. H., & Scott, P. F. 1965, MmRAS, 69, 183

Prestage, R.M., & Peacock, J.A. 1988, MNRAS, 230, 131

Prestage, R.M., & Peacock, J.A. 1989, MNRAS, 236, 959

Rector, T., Stocke, J.T., & Ellingson, E. 1995, AJ, 110, 1492

Roos, N. 1981, A&A, 104, 218

Roos, N. 1985, ApJ, 294, 479

Sebok, W.L. 1986, ApJS, 62, 301

Seldner, M., & Peebles, P.J.E. 1978, ApJ, 225, 7

Smith, E.P., Heckman, T.M., Bothun, G.D., Romanishin, W., & Balick, B. 1986, ApJ, 306, 64

Smith, H.E., Spinrad, H., & Smith, E.O. 1976, PASP, 88, 621

Spinrad, H., Djorgovski, S., Marr, J., & Aguilar, L. 1985, PASP, 97, 932

Spinrad, H., et al. 1991, electronic version of The Revised 3C Catalog of Radio Sources.

Stocke, J.T., Perlman, E.S., Gioia, I.M., & Harvanek, M. 1999, AJ, 117, 1967

Stocke, J.T., & Perrenod, S.C. 1981, ApJ, 245, 375

Stockton, A., & MacKenty, J.W. 1987, ApJ, 316, 584

Tadhunter, C. N., Morganti, R., di Serego-Alighieri, S., Fosbury, R. A. E., & Danziger, I. J. 1993, MNRAS, 263, 9

Wilson, A.S., & Colbert, E.J.M. 1995, ApJ, 486, 62

Wold, M., Lacy, M., Lilje, P.B., & Serjeant, S. 2000, MNRAS, 316, 267

Worrall, D.M. 1987, in Superluminal Radio Sources, ed. J.A. Zensus and T.J. Pearson (Cambridge: Cambridge University Press), 251

Wurtz, R., Stocke, J.T., Ellingson, E., & Yee, H.K.C. 1997, ApJ, 480, 547

Wyndham, J.D. 1966, ApJ, 144, 459

Yates, M.G., Miller, L., & Peacock, J.A. 1989, MNRAS, 240, 129 (YMP)

Yee, H.K.C. 1991, PASP, 103, 396

Yee, H.K.C., & Ellingson, E. 1993, ApJ, 411, 43 (YE93)

Yee, H.K.C., Ellingson, E., & Carlberg, R. G. 1996, ApJS, 102, 269

Yee, H.K.C., & Green, R.F. 1984, ApJ, 280, 79

Yee, H.K.C., & Green, R.F. 1987, ApJ, 319, 28 (YG)

Yee, H.K.C., Green, R.F., & Stockman, H.S. 1986, ApJS, 62, 681

Yee, H.K.C., & López-Cruz, O. 1999, AJ, 117, 1985

Zamorani, G., et al. 1981, ApJ, 245, 357

Zirbel, E.L. 1997, ApJ, 476, 489

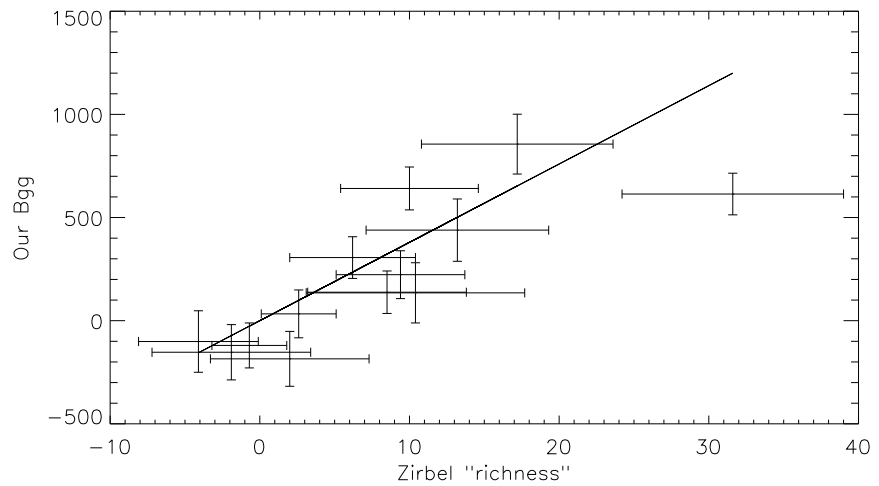


Fig. 1.— The data points with 1σ error bars and the weighted linear fit that is the conversion from Zirbel (1997) “richness” values ($N_{0.5}^{-19}$) to B_{gg} . The fit has been forced through the point (0,0). The resulting conversion is $B_{gg} = 38N_{0.5}^{-19}$.

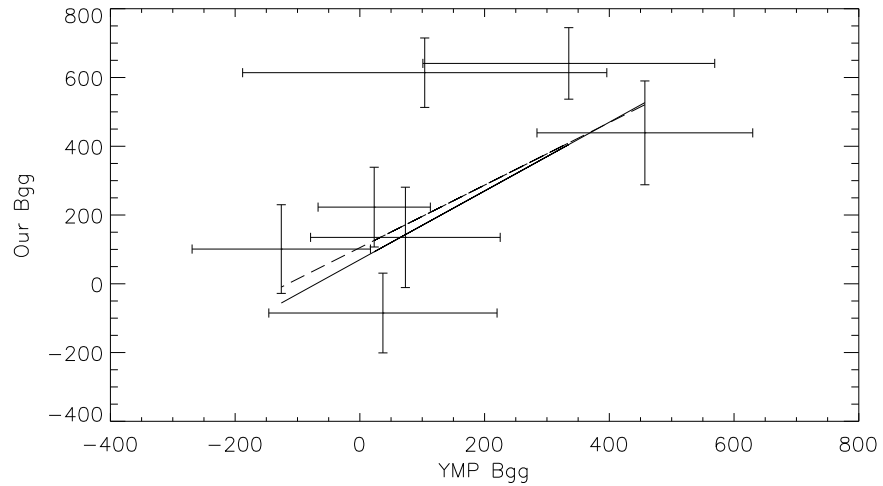


Fig. 2.— The data points with 1σ error bars and two possible fits for the conversion from Yates, Miller & Peacock (1989; YMP) B_{gg} values to our B_{gg} values. The solid line is the conversion based on the average offsets of the data points (i.e., a forced slope of unity). The dashed line is a weighted least squares linear fit. The two fits agree to within their errors. The two uppermost data points were not used in the calculation of either fit (for reasons given in the text). The average offset fit (the solid line; $B_{gg} = \text{YMP } B_{gg} + 70$) was used for the conversion.

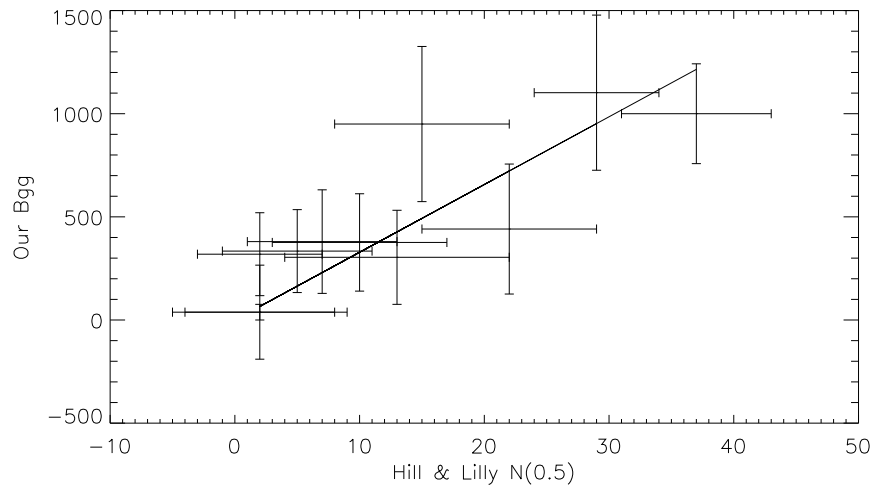


Fig. 3.— The data points with 1σ error bars and the weighted linear fit that is the conversion from Hill & Lilly (1991; HL) $N_{0.5}^M$ values to B_{gg} . The fit has been forced through the point $(0,0)$. The resulting conversion is $B_{gg} = 33N_{0.5}^M$. This fit agrees quite well with the conversions discussed in HL.

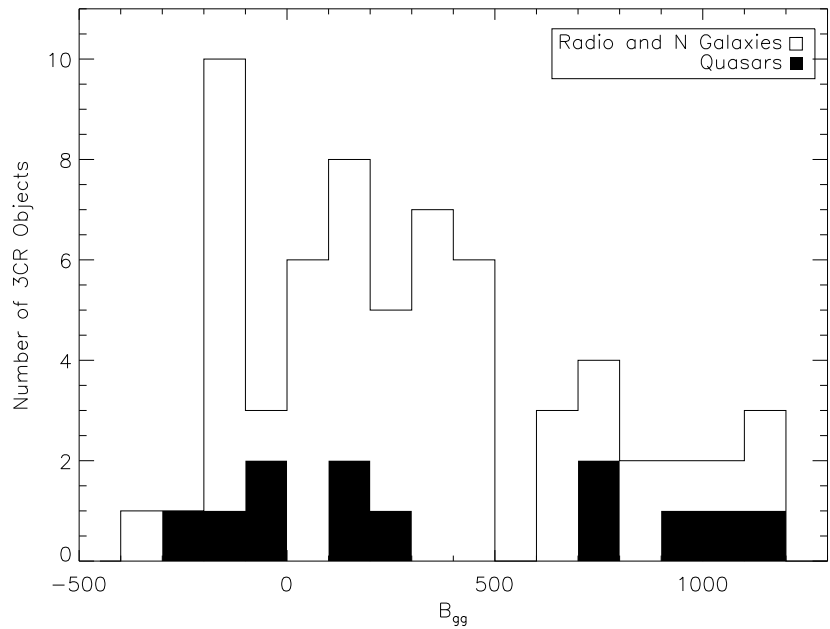


Fig. 4.— A histogram showing the distribution of B_{gg} values. The open blocks are the radio galaxies and N-galaxies; the shaded blocks are the quasars. The two objects with a very large discrepancy between B_{gg} values found by other investigations (3C 275 and 3C 435A) are not included in the distribution.

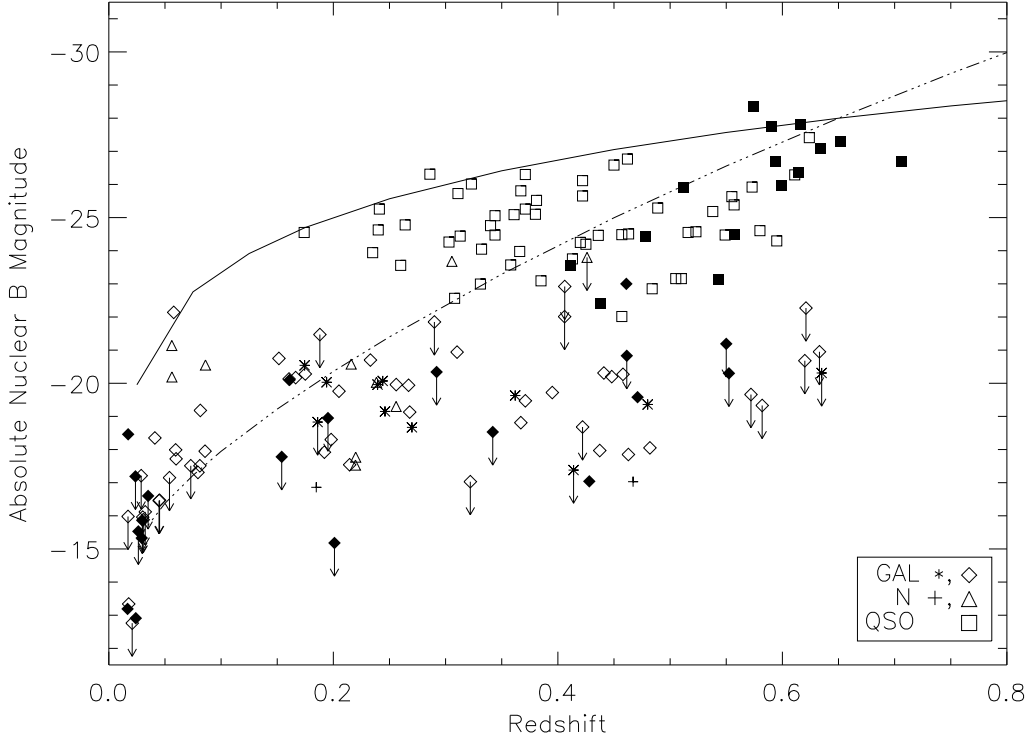


Fig. 5.— Nuclear M_B vs. z for radio galaxies, N-galaxies and quasars. The absolute magnitudes are in rest-frame Johnson B and have been corrected for Galactic reddening. The radio galaxies appear as diamonds, the N-galaxies as triangles and the quasars as squares. Sources that are located in rich environments ($B_{gg} > 500 \text{ Mpc}^{1.77}$) are denoted by filled symbols while those in poor environments ($B_{gg} \leq 500 \text{ Mpc}^{1.77}$) are marked with open symbols. For some sources the environment is unknown and these are marked with either an asterisk (radio galaxies) or a plus sign (N-galaxies). Symbols with an arrow indicate that the absolute nuclear B magnitude is an upper limit. The $z = 0.15 - 0.65$ radio and N-galaxies are from the present work, the lower redshift galaxies are from Yee & Ellingson (1993) and the quasars are originally from Ellingson, Yee & Green (1991; EYG). Model curves for the upper envelope of the points are derived from an AGN luminosity function, using a “standard $\kappa_L = 3.7$ model” (solid line), matching the upper envelope for all objects, and a $\kappa_L = 19$ model (dot-dashed line) describing the upper envelope for the quasars and radio galaxies in rich environments (see text for details).

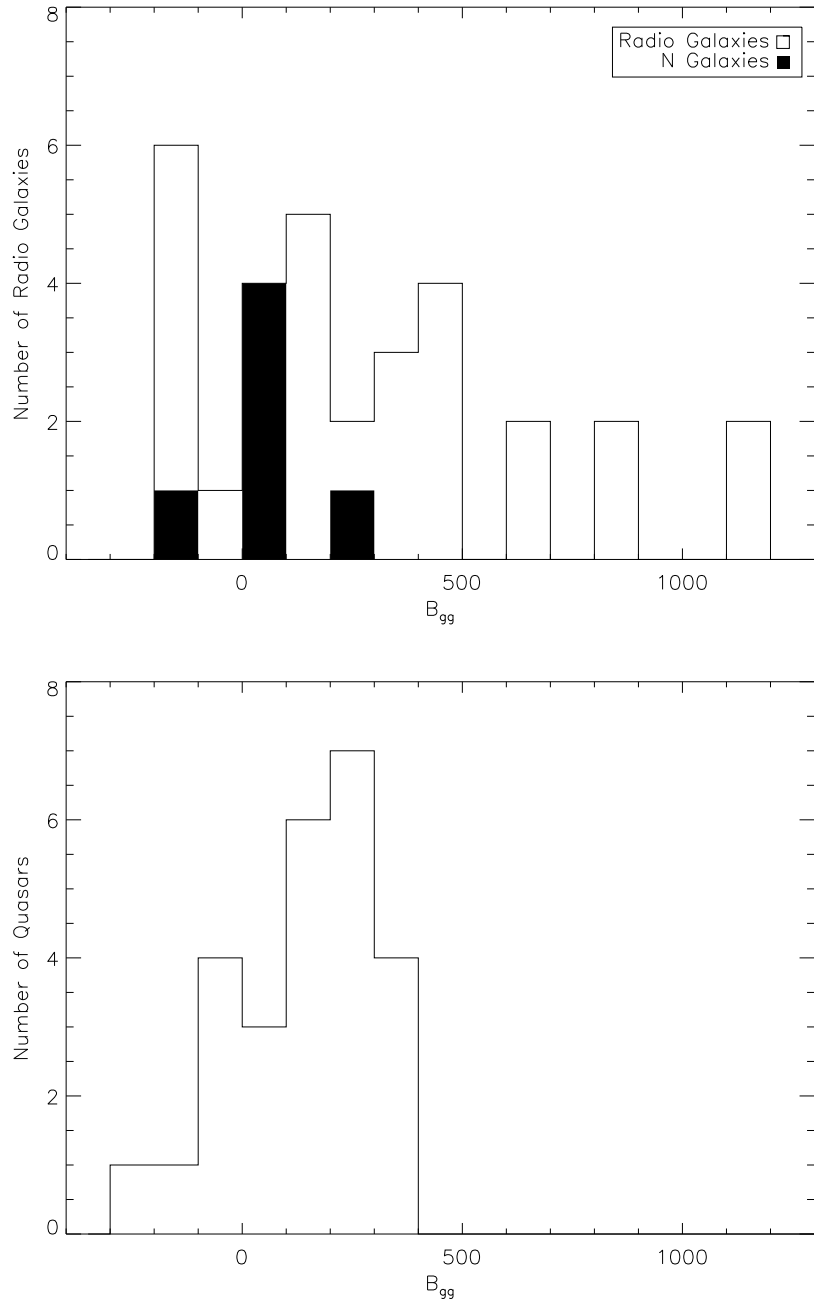


Fig. 6.— a)The distribution of B_{gg} values for the galaxy environments of radio galaxies and N-galaxies with $0.15 < z < 0.4$. The N-galaxies are the shaded blocks. b) The distribution of B_{gg} values for the galaxy environments of quasars with $0.15 < z < 0.4$. A KS-test gives only a 3% chance that these two distributions come from the same parent population. If the N-galaxies are grouped with the quasars, the probability is 0.4%.

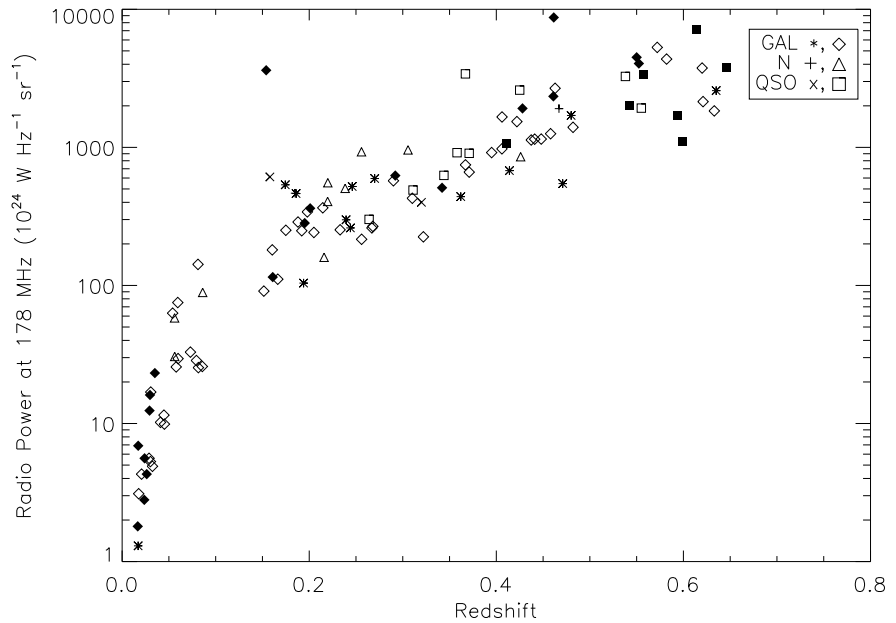


Fig. 7.— Total P_{178} vs. z for all 3CR objects (both galaxies and quasars) used in this study (including the radio galaxies with $z < 0.1$ taken from Yee & Ellingson 1993). The radio power is the total power emitted in the rest frame at 178 MHz. The symbols have the same meaning as in Figure 5. Two additional quasars with unknown environments are marked with an “X”.

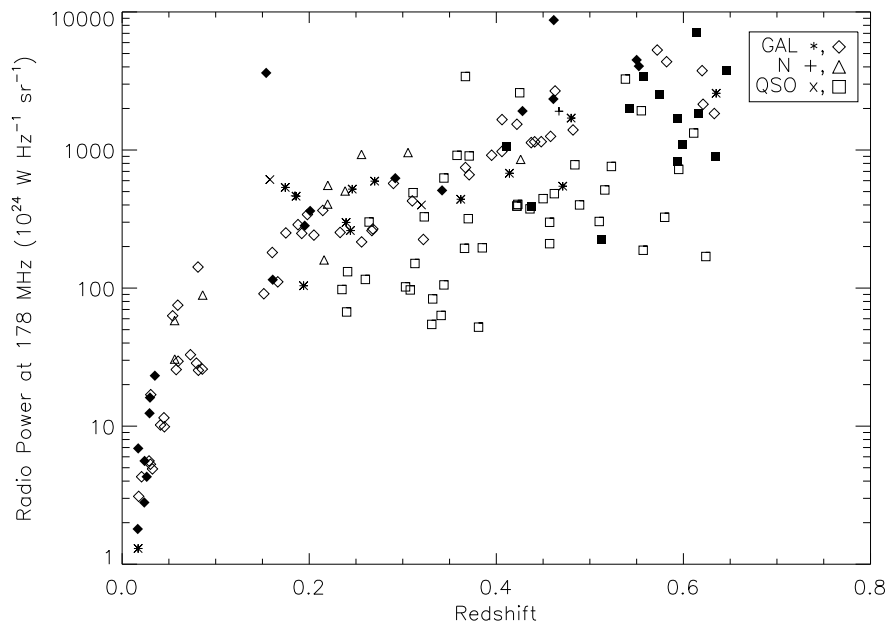


Fig. 8.— Same as Figure 7, but includes all objects in the combined radio galaxy and quasar samples.

Table 1: The Sample of 3CR Sources

Source (3CR#)	R.A. (B1950.)	Dec. (B1950.)	z	S_{178} (Jy)	α_{178}^{750}	$P_{178} (10^{24}$ W Hz $^{-1}$ sr $^{-1}$)	$\log P_{178}$	Optical Class	ID
16.0	00 35 09.16	13 03 39.6	0.406	12.2	0.94	976	26.99	N	GAL
17.0	00 35 47.18	-02 24 09.5	0.2197	21.8	0.55	406	26.61	B	N
18.0	00 38 14.57	09 46 56.1	0.188	20.7	0.76	288	26.46	N	GAL
19.0	00 38 13.76	32 53 39.9	0.482	13.2	0.63	1398	27.15	N?	GAL
28.0	00 53 09.12	26 08 23.4	0.1952	17.8	1.06	283	26.45	—	GAL
42.0	01 25 42.67	28 47 30.4	0.395	13.1	0.73	917	26.96	N	GAL
46.0	01 32 34.09	37 38 47.0	0.4373	11.1	1.13	1131	27.05	N	GAL
47.0	01 33 40.42	20 42 10.6	0.425	28.8	0.98	2600	27.41	B	QSO
48.0	01 34 49.82	32 54 20.4	0.367	60.0	0.59	3409	27.53	—	QSO
49.0	01 38 28.41	13 38 19.9	0.621	11.2	0.65	2145	27.33	—	GAL
61.1	02 10 37.1	86 05 18.5	0.186	34.0	0.77	463	26.67	E	GAL
63.0	02 18 21.90	-02 10 33.	0.175	20.9	0.81	251	26.40	N	GAL
67.0	02 21 18.05	27 36 37.4	0.3102	10.9	0.58	428	26.63	—	GAL
79.0	03 07 11.48	16 54 36.9	0.2559	33.2	0.92	930	26.97	N	N
93.0	03 40 51.54	04 48 21.7	0.358	15.7	0.85	915	26.96	B	QSO
93.1	03 45 35.80	33 44 05.9	0.244	10.8	0.73	261	26.42	—	GAL
99.0	03 58 33.28	00 28 10.6	0.426	9.6	0.93	856	26.93	—	N
109.0	04 10 54.85	11 04 39.5	0.3056	23.5	0.85	959	26.98	B	N
142.1	05 28 48.1	06 28 14.8	0.4061	21.1	0.89	1661	27.22	—	GAL
169.1	06 47 35.5	45 13 01.	0.633	8.0	0.93	1838	27.26	N	GAL
171.0	06 51 11.05	54 12 50.0	0.2384	21.3	0.87	505	26.70	N	N
173.1	07 02 47.91	74 54 16.6	0.292	16.8	0.88	625	26.80	E	GAL
196.1	08 12 57.32	-02 59 13.9	0.198	20.3	1.19	341	26.53	—	GAL
200.0	08 24 21.43	29 28 42.2	0.458	12.3	0.84	1256	27.10	E	GAL
213.1	08 58 05.15	29 13 34.5	0.194	7.2	0.58	104	26.02	N	GAL
215.0	09 03 44.15	16 58 15.7	0.411	12.4	1.06	1064	27.03	B	QSO
219.0	09 17 50.70	45 51 44.2	0.1744	44.9	0.81	536	26.73	B	GAL
220.1	09 26 31.87	79 19 45.4	0.620	17.2	0.93	3756	27.57	N	GAL
225.0B	09 39 32.19	13 59 33.3	0.582	23.2	0.94	4362	27.64	N?	GAL
228.0	09 47 27.72	14 34 02.9	0.5524	23.8	1.00	4050	27.61	N	GAL
234.0	09 58 57.38	29 01 37.4	0.1848	34.2	0.86	466	26.67	N/B?	N
244.1	10 30 19.61	58 30 04.3	0.428	22.1	0.82	1916	27.28	N	GAL
249.1	11 00 27.42	77 15 08.7	0.311	11.7	0.81	491	26.69	B	QSO
258.0	11 22 06.42	19 35 58.8	3.7	0.60					
263.0	11 37 08.97	66 04 26.9	0.646	16.6	0.82	3795	27.58	B	QSO
268.2	11 58 24.8	31 50 02.	0.362	7.5	0.79	440	26.64	N	GAL
268.3	12 03 54.28	64 30 18.6	0.371	11.7	0.50	662	26.82	—	GAL
273.0	12 26 33.35	02 19 42.0	0.158	68.5	0.26	611	26.79	B	QSO
274.1	12 32 56.74	21 37 05.8	0.422	18.0	0.87	1537	27.19	E?	GAL
275.0	12 39 45.16	-04 29 53.9	0.480	15.8	0.70	1704	27.23	E	GAL
275.1	12 41 27.58	16 39 18.0	0.557	19.9	0.96	3394	27.53	B	QSO
277.0	12 49 26.15	50 50 42.9	0.414	8.2	0.91	679	26.83	E?	GAL
277.1	12 50 15.13	56 50 36.4	0.320	9.3	0.67	400	26.60	—	QSO
284.0	13 08 41.38	27 44 02.6	0.2394	12.3	0.95	299	26.48	N	GAL
287.1	13 30 20.46	02 16 09.0	0.2159	8.9	0.55	160	26.20	B	N
288.0	13 36 38.59	39 06 21.8	0.246	20.6	0.85	521	26.72	—	GAL
295.0	14 09 33.44	52 26 13.6	0.4614	91.0	0.63	8730	27.94	—	GAL
299.0	14 19 06.29	41 58 30.2	0.367	12.9	0.65	747	26.87	—	GAL
300.0	14 20 40.10	19 49 13.2	0.270	19.5	0.78	595	26.77	N	GAL
303.1	14 43 53.7	77 20 05.	0.267	8.8	0.77	261	26.42	—	GAL
306.1	14 52 24.5	-04 08 47.	0.441	12.4	0.81	1147	27.06	N	GAL
313.0	15 08 32.66	08 02 48.2	0.461	22.5	0.85	2342	27.37	N	GAL
319.0	15 22 43.90	54 38 38.4	0.192	16.7	0.90	249	26.40	E	GAL
320.0	15 29 29.70	35 43 48.5	0.342	9.9	0.78	510	26.71	E	GAL
323.1	15 45 31.11	21 01 32.5	0.264	10.6	0.68	301	26.48	B	QSO
327.1	16 02 12.96	01 25 58.7	0.4628	25.7	0.83	2679	27.43	N	GAL
330.0	16 09 13.90	66 04 22.8	0.550	30.3	0.71	4492	27.65	N	GAL
332.0	16 15 47.27	32 29 45.0	0.1515	10.5	0.64	91	25.96	B	GAL
334.0	16 18 07.40	17 43 30.5	0.555	11.9	0.86	1925	27.28	B	QSO
337.0	16 27 19.07	44 25 38.2	0.635	12.9	0.63	2577	27.41	N	GAL
341.0	16 26 02.4	27 48 14.	0.448	11.8	0.85	1149	27.06	N	GAL
345.0	16 41 17.60	39 54 10.7	0.594	11.8	0.27	1706	27.23	B	QSO
346.0	16 41 34.56	17 21 20.7	0.161	11.9	0.52	115	26.06	—	GAL
348.0	16 48 39.98	05 04 35.0	0.154	382.6	1.03	3619	27.56	E	GAL
349.0	16 58 04.44	47 07 20.3	0.205	14.5	0.74	242	26.38	N	GAL
351.0	17 04 03.51	60 48 31.3	0.371	14.9	0.73	906	26.96	B	QSO
357.0	17 26 27.41	31 48 23.9	0.1664	10.6	0.59	111	26.04	N	GAL
379.1	18 25 55.93	74 19 06.8	0.256	8.1	0.70	216	26.33	N	GAL
381.0	18 32 24.40	47 24 36.5	0.1605	18.1	0.81	181	26.26	B	GAL
401.0	19 39 38.84	60 34 32.6	0.201	22.8	0.71	362	26.56	E	GAL
411.0	20 19 44.19	09 51 33.8	0.467	18.0	0.82	1909	27.28	N	N
427.1	21 04 44.80	76 21 09.5	0.572	29.0	0.97	5300	27.72	E	GAL
434.0	21 20 54.40	15 35 11.7	0.322	5.2	0.64	225	26.35	E	GAL
435.0A	21 26 37.01	07 19 52.4	0.471	4.9	0.90	547	26.74	N	GAL
436.0	21 41 57.91	27 56 30.3	0.2145	19.4	0.86	365	26.56	N	GAL
455.0	22 52 34.53	12 57 33.5	0.5427	14.0	0.71	2012	27.30	—	QSO
456.0	23 09 56.65	09 03 07.8	0.2330	11.6	0.72	253	26.40	N	GAL
458.0	23 10 21.9	05 00 26.	0.290	15.8	0.84	573	26.76	N	GAL
459.0	23 14 02.27	03 48 55.2	0.2199	27.9	0.87	555	26.74	N	N
460.0	23 18 59.75	23 30 20.4	0.268	8.9	0.80	268	26.43	N	GAL

Table 2: Optical Observations

Source (3CR#)	Filter	UT Date	Telescope	Integration Time (sec)	Seeing (arcsec)	5 σ Limiting Magnitude
16.0	r	06NOV96	2.1 m	1800	1.3	23.88
	g	07NOV96	2.1 m	3600	1.6	24.36
17.0	r	09NOV96	2.1 m	900	0.9	23.58
	g	09NOV96	2.1 m	1800	1.2	24.09
18.0	r	08NOV96	2.1 m	900	1.4	23.13
	g	06NOV96	2.1 m	1800	1.5	24.05
19.0	r	05NOV96	2.1 m	1800	1.0	24.11
	g	08NOV96	2.1 m	3600	1.7	24.28
28.0	r	06NOV96	2.1 m	900	1.5	23.29
	g	08NOV96	2.1 m	1800	1.4	23.88
42.0	r	05NOV96	2.1 m	1800	0.9	24.20
	g	08NOV96	2.1 m	3600	1.4	24.45
46.0	r	09NOV96	2.1 m	1800	0.9	24.03
	r	08NOV96	2.1 m	1800	1.4	23.64
47.0	g	09NOV96	2.1 m	3600	1.1	24.56
	r	05NOV96	2.1 m	2700	0.8	24.27
49.0	g	07NOV96	2.1 m	4500	1.3	24.62
	r	06NOV96	2.1 m	1800	1.3	23.76
67.0	g	09NOV96	2.1 m	2700	1.5	24.10
	r	09NOV96	2.1 m	1260	1.7	23.26
79.0	g	09NOV96	2.1 m	2700	1.5	24.07
	r	06NOV96	2.1 m	1800	1.2	23.78
93.0	g	08NOV96	2.1 m	3600	1.7	24.13
	r	05NOV96	2.1 m	1800	1.0	23.99
99.0	r	05NOV96	2.1 m	3600	1.3	24.61
	g	07NOV96	2.1 m	1800	1.6	23.54
109.0	g	06NOV96	2.1 m	3600	1.5	24.35
	r	07NOV96	2.1 m	1800	1.3	23.52
142.1	r	09NOV96	2.1 m	2700	0.9	24.17
	r	05NOV96	2.1 m	4500	1.6	24.34
169.1	g	08NOV96	2.1 m	600	1.0	23.24
	r	07NOV96	2.1 m	1800	1.4	24.01
171.0	r	05NOV96	2.1 m	1800	1.2	23.55
	g	09NOV96	2.1 m	2160	1.2	24.21
173.1	r	05NOV96	2.1 m	2700	1.4	23.77
	g	08NOV96	2.1 m	4500	1.8	24.12
220.1	r	05NOV96	2.1 m	1800	1.3	22.61
	g	03JUL94	0.9 m	3600	1.6	23.46
303.1	r	03JUL94	0.9 m	1800	1.3	22.95
	g	03JUL94	0.9 m	3600	1.3	23.74
319.0	r	02JUL94	0.9 m	1800	1.5	22.94
	g	02JUL94	0.9 m	4500	1.5	23.60
320.0	r	02JUL94	0.9 m	2700	1.5	22.49
	g	02JUL94	0.9 m	1800	1.7	22.83
323.1	r	06JUL94	0.9 m	3600	1.3	22.68
	g	06JUL94	0.9 m	1800	1.0	23.40
332.0	r	04JUL94	0.9 m	3600	1.6	22.94
	g	04JUL94	0.9 m	1800	1.8	23.50
346.0	r	04JUL94	0.9 m	3600	1.6	22.83
	g	04JUL94	0.9 m	1800	1.7	23.40
348.0	r	06JUL94	0.9 m	3600	1.8	22.79
	g	06JUL94	0.9 m	1800	1.8	23.23
349.0	r	03JUL94	0.9 m	3600	1.2	23.09
	g	03JUL94	0.9 m	1800	1.4	23.69
351.0	r	09NOV96	2.1 m	3600	1.0	23.86
	g	09NOV96	2.1 m	2700	1.1	24.26
357.0	r	02JUL94	0.9 m	1800	1.4	22.98
	g	02JUL94	0.9 m	3600	1.5	23.38
379.1	r	05JUL94	0.9 m	1800	1.9	22.77
	g	05JUL94	0.9 m	3600	2.0	23.22
381.0	r	03JUL94	0.9 m	1800	1.3	23.04
	g	03JUL94	0.9 m	3600	1.5	23.38
401.0	r	04JUL94	0.9 m	1800	1.6	22.91
	g	04JUL94	0.9 m	3600	1.8	23.28
427.1	r	06NOV96	2.1 m	2700	1.4	23.68
	g	07NOV96	2.1 m	3600	1.5	24.47
434.0	r	05JUL94	0.9 m	2340	2.0	22.67
	g	05JUL94	0.9 m	4320	2.2	23.29
436.0	r	04JUL94	0.9 m	1800	1.8	22.63
	g	04,06JUL94	0.9 m	2700	1.7	23.13
456.0	r	08NOV96	2.1 m	900	1.1	23.25
	g	08NOV96	2.1 m	1800	1.6	23.89
458.0	r	05JUL94	0.9 m	1800	1.9	22.74
	g	05,06JUL94	0.9 m	3600	2.0	23.01
459.0	r	08NOV96	2.1 m	900	1.6	23.11
	g	08NOV96	2.1 m	1800	1.8	23.65
460.0	r	03JUL94	0.9 m	2100	1.8	22.66
	g	06JUL94	0.9 m	2700	1.9	23.07

Table 3: Radio Galaxy Magnitudes and Colors

Source (3CR#)	z	Total m_r	Observed $g - r$	Total M_r	Total M_g	Nuclear M_r	Nuclear M_B
16.0	0.406	20.07	1.31	-22.86	-22.75		
17.0	0.2197	18.05	0.54	-23.07	-23.06	-17.67	-17.53
18.0	0.188	18.82	0.47	-21.90	-21.85		
19.0	0.482	19.89	1.45	-23.78	-23.49	-18.20	-18.05
28.0	0.1952	17.41	0.88	-23.41	-22.97	> -19.09	> -18.95
42.0	0.395	19.42	1.33	-23.49	-23.37	-19.86	-19.72
46.0	0.4373	18.98		-24.31		-18.11	-17.97
49.0	0.621	20.84	1.11	-24.00	-23.87		
61.1	0.186	20.70:				>-18.98	> -18.83
63.0	0.175	18.20:		-22.30:		-20.42	-20.28
67.0	0.3102	18.86	1.07	-23.31	-23.18	-21.08	-20.94
79.0	0.2559	17.62	1.20	-24.08	-23.63	-19.45	-19.30
93.1	0.244	19.63:		-22.21:		-20.21	-20.07
99.0	0.426	18.70	0.87	-24.72	-25.15		
109.0	0.3056	17.10	0.93	-25.53	-25.72	-23.82	-23.68
142.1	0.4061	19.97		-23.77			
169.1	0.633	20.62	0.92	-24.55	-24.70		
171.0	0.2384	18.23	0.89	-23.20	-22.96	-20.17	-20.03
173.1	0.292	17.70	1.27	-24.29	-23.90	>-20.48	>-20.34
196.1	0.198	18.09:		-22.84:		-18.45	-18.30
200.0	0.458	20.43:		-22.96:		>-20.41	> -20.27
213.1	0.194	16.98:		-23.78:		-20.18	-20.03
219.0	0.1744	18.34:		-22.11:		-20.69	-20.54
220.1	0.620	20.55	0.89	-24.28	-24.37		
234.0	0.1848	17.97:		-22.67:		-17.01	-16.86
244.1	0.428	19.64:		-23.41:		-17.18	-17.04
268.2	0.362	19.63:		-22.85:		-19.77	-19.63
268.3	0.371	20.41:		-22.15:		-19.61	-19.47
274.1	0.422	20.32:		-22.74:		>-18.83	>-18.68
275.0	0.480	21.32:		-22.22:		>-19.50	>-19.36
277.0	0.414	20.24:		-22.68:		>-17.52	>-17.38
284.0	0.2394	18.59:		-22.72:		-20.11	-19.96
287.1	0.2159	18.49:		-22.54:		-20.72	-20.58
288.0	0.246	17.91:		-23.45:		-19.29	-19.15
299.0	0.367	21.48:		-21.04:		-18.96	-18.81
300.0	0.270	18.41:		-23.21:		-18.82	-18.67
303.1	0.267	18.19	1.04	-23.47	-23.17	-20.08	-19.94
306.1	0.441	20.02:		-23.30:		-20.45	-20.31
313.0	0.461	19.25:		-24.13:		-23.15	-23.00
319.0	0.192	18.67	0.81	-22.07	-21.68	>-18.06	>-17.92
320.0	0.342	18.52	1.55	-23.83	-23.29	>-18.68	>-18.53
327.1	0.4628	20.53:		-23.05:		-17.99	-17.85
332.0	0.1515	17.03	0.63	-23.10	-22.78	-20.90	-20.75
341.0	0.448	21.50:		-21.80:		-20.34	-20.20
346.0	0.161	17.40	0.92	-23.04	-22.52	-20.24	-20.10
348.0	0.154	16.75	0.83	-23.61	-23.17	>-17.93	>-17.78
349.0	0.205	18.28	0.97	-22.59	-22.07	-19.91	-19.76
357.0	0.1664	16.73	0.93	-23.71	-23.16	-20.32	-20.17
379.1	0.256	17.79	1.07	-23.84	-23.50	-20.11	-19.96
381.0	0.1605	17.61	0.81	-22.78	-22.35	-20.27	-20.13
401.0	0.201	17.78	0.92	-23.23	-22.81	>-15.33	>-15.18
411.0	0.467	21.81:		-22.05:		-17.17	-17.03
427.1	0.572	21.28	1.81	-23.52	-22.87		
434.0	0.322	19.26	1.40	-23.10	-22.72	>-17.17	>-17.03
435.0A	0.471	22.02:		-21.52:		-19.73	-19.58
436.0	0.2145	17.91	1.02	-23.35	-22.93	-17.69	-17.54
456.0	0.2330	18.20	0.88	-23.09	-22.80	-20.84	-20.70
458.0	0.290	19.44	1.28	-22.46	-22.02		
459.0	0.2199	17.43	0.21	-23.71	-24.04	-17.92	-17.77
460.0	0.268	18.61	0.83	-23.10	-23.17	-19.28	-19.13

Table 4: Quasar Magnitudes and Colors

Source (3CR#)	z	Total m_r	Observed $g - r$	Total M_r	Total M_g	Total M_B
47.0	0.425	17.90	-0.20	-24.47	-24.72	-24.33
93.0	0.358	18.29	0.49	-23.95	-23.60	-23.80
323.1	0.264	16.21	0.14	-25.01	-24.90	-24.86
351.0	0.371	15.47	-0.02	-26.46	-26.48	-26.32

Table 5: Comparison of Excess Galaxy Measurement Methods

Method	Tabulated Quantity	H_0 ($\text{km s}^{-1} \text{Mpc}^{-1}$)	q_0	Optical Waveband	Counting Area	m_{lim}	Background Counts	Stars vs. Galaxies?	Other Notes
Ours	B_{gg}	50	0.02	Gunn r	0.5 Mpc radius	m_{comp} or $M_r^*(z) + 2.5$	YGS+Y	Yes	
YE	B_{gg}	50	0.02, 0.5	Gunn r	0.5 Mpc radius	m_{comp} or $M_r^*(z) + 2.5$	YGS	Yes	1
Z	$N_{-19}^{0.5}$	50	0	V	0.5 Mpc radius	$M_V = -19$	20'-60' offset	Yes	2
YMP	B_{gg}	50	0	R_c to Gunn r	variable	m_{comp}	5'-10' offset	No	3
HL	$N_{0.5}^M$	50	0.5	R	0.5 Mpc radius	$m_1 + 3$	30' offset	No	

Note. —

- (1) Some fields done using the luminosity function of Sebok 1986 and $q_0 = 0.5$.
- (2) No galaxies with “anomalous” colors.
- (3) Different definition of the completeness limit, m_{comp} from YE and this paper.

References. —

HL: Hill & Lilly (1991);
 Y: Yee, private communication;
 YE: Yee & Ellingson (1993);
 YGS: Yee, Green & Stockman (1986);
 YMP: Yates, Miller & Peacock (1989);
 Z: Zirbel (1997).

Table 6: B_{gg} Values

3CR #	z	Ours	YE	Z	Z2	HL	YMP	Notes
16.0	0.406	439 \pm 151		502 \pm 232			527 \pm 173	
17.0	0.2197	223 \pm 116		357 \pm 163			93 \pm 90	
18.0	0.188	-120 \pm 109		-27 \pm 95				
19.0	0.482	249 \pm 170						
28.0	0.1952	1179 \pm 110						
42.0	0.395	-101 \pm 149		-156 \pm 152				
46.0	0.4373	341 \pm 158						
47.0	0.425	-119 \pm 157						
48.0	0.367		108 \pm 118					
49.0	0.621	232 \pm 252						
63.0	0.175			441 \pm 163				
67.0	0.3102	-153 \pm 134		-72 \pm 201				
79.0	0.2559	90 \pm 126						
93.0	0.358	-252 \pm 144						
99.0	0.426	-169 \pm 155						
109.0	0.3056	-185 \pm 133		76 \pm 201				
142.1	0.4061	54 \pm 161						
169.1	0.633	-312 \pm 302						
171.0	0.2384	57 \pm 118						
173.1	0.292	806 \pm 129						
196.1	0.198		448 \pm 175					
200.0	0.458			38 \pm 228 (Z)	66 \pm 198			
215.0	0.411		1000 \pm 242		1221 \pm 198			
220.1	0.620	418 \pm 330						
225.0B	0.582					185 \pm 574	1	
228.0	0.5524					594 \pm 495	1230 \pm 468	2
244.1	0.428			950 \pm 376 (Z)	495 \pm 231			3
249.1	0.311	-38 \pm 141						
263.0	0.646	993 \pm 550						
268.3	0.371			304 \pm 228 (Z)	429 \pm 297			
274.1	0.422			380 \pm 251 (Z)	231 \pm 198	362 \pm 129	4	
275.0	0.480			38 \pm 38 (Z)	66 \pm 231	669 \pm 183	5	
275.1	0.557	1125 \pm 399						
287.1	0.2159		76 \pm 99					
295.0	0.4614			1102 \pm 376 (Z)	957 \pm 165		6	
299.0	0.367		319 \pm 201	152 \pm 228 (AEZO)	66 \pm 165		7	
303.1	0.267	115 \pm 128						
306.1	0.441		334 \pm 201	190 \pm 380 (AEZO)	165 \pm 198	529 \pm 115	8	
313.0	0.461		441 \pm 315	1064 \pm 532 (AEZO)	726 \pm 231		9	
319.0	0.192	494 \pm 109						
320.0	0.342	856 \pm 145		654 \pm 243				
323.1	0.264	268 \pm 127	440 \pm 224					
327.1	0.4628					-195 \pm 181	10	
330.0	0.550				660 \pm 231			
332.0	0.1515	306 \pm 101		236 \pm 160				
334.0	0.555		187 \pm 220					
341.0	0.448			376 \pm 236	266 \pm 380 (AEZO)	330 \pm 231		
345.0	0.594		773 \pm 297					
346.0	0.161	641 \pm 104		380 \pm 175		405 \pm 234		
348.0	0.154	614 \pm 101		1201 \pm 281		174 \pm 292	11	
349.0	0.205	206 \pm 112						
351.0	0.371	-82 \pm 146	-198 \pm 138					
357.0	0.1664	370 \pm 103						
379.1	0.256	-136 \pm 126						
381.0	0.1605	138 \pm 103		323 \pm 201				
401.0	0.201	1131 \pm 112						
427.1	0.572	-166 \pm 289						
434.0	0.322	135 \pm 146		395 \pm 277		143 \pm 152		
435.0A	0.471			1273 \pm 308		573 \pm 227	12	
436.0	0.2145	420 \pm 115						
455.0	0.5427		764 \pm 366					
456.0	0.2330	-85 \pm 116				107 \pm 183		
458.0	0.290	101 \pm 129				-56 \pm 143		
459.0	0.2199	33 \pm 116		99 \pm 95				
460.0	0.268	-110 \pm 128						

Note. —

(1) The YMP counting area (A_{YMP}) is $1.4 \times$ the area given by a 0.5 Mpc radius ($A_{r=0.5Mpc}$).

(2) The error bars overlap but the difference between the two values is substantial. The HL value is uncertain due to a large ($>$ a factor of 2) correction due to a “bright” m_{lim} . The YMP m_{lim} is even brighter and $A_{YMP} = 1.3 \times A_{r=0.5Mpc}$.

(3) The error bars overlap but the difference between the two values is substantial. HL suggest the comparison field had higher counts than it should have.

(4) The error bars overlap. HL $m_{lim} = 22$. YMP $m_{lim} = 23.51$. $A_{YMP} = 2.6 \times A_{r=0.5Mpc}$.

(5) The two smaller values agree with each other but are highly discrepant with the larger value. HL $m_{lim} = 23$. YMP $m_{lim} = 22.88$. $A_{YMP} = 2.3 \times A_{r=0.5Mpc}$.

Table 7: Adopted B_{gg} Values

Source (3CR#)	z	ID	B_{gg} (Mpc $^{1.77}$)	σ (Mpc $^{1.77}$)	References	Notes
16.0	0.406	GAL	439	151		
17.0	0.2197	N	223	116		
18.0	0.188	GAL	-120	109		
19.0	0.482	GAL	249	170		
28.0	0.1952	GAL	1179	110		
42.0	0.395	GAL	-101	149		
46.0	0.4373	GAL	341	158		
47.0	0.425	QSO	-119	157		
48.0	0.367	QSO	108	118	YE	
49.0	0.621	GAL	232	252		
63.0	0.175	GAL	441	163	Z	
67.0	0.3102	GAL	-153	134		
79.0	0.2559	N	90	126		
93.0	0.358	QSO	-252	144		
99.0	0.426	N	-169	155		
109.0	0.3056	N	-185	133		
142.1	0.4061	GAL	54	161		
169.1	0.633	GAL	-312	302		
171.0	0.2384	N	57	118		
173.1	0.292	GAL	806	129		
196.1	0.198	GAL	448	175	Z	
200.0	0.458	GAL	52	213	avg. of Z2(Z) and HL	
215.0	0.411	QSO	1000	242	YE	
220.1	0.620	GAL	418	330		
225.0B	0.582	GAL	185	574	YMP	
228.0	0.5524	GAL	912	482	avg. of HL and YMP	
244.1	0.428	GAL	723	304	avg. of Z2(Z) and HL	
249.1	0.311	QSO	-38	141	YE	
263.0	0.646	QSO	993	550	YE	
268.3	0.371	GAL	367	263	avg. of Z2(Z) and HL	
274.1	0.422	GAL	324	193	avg. of Z2(Z), HL and YMP	
275.0	0.480	GAL	38-669		Z2(Z), YMP	
275.1	0.557	QSO	1125	399	YE	
287.1	0.2159	N	76	99	Z	
295.0	0.4614	GAL	1030	271	avg. of Z2(Z) and HL	
299.0	0.367	GAL	179	198	avg. of Z, Z2(AEZO) and HL	
303.1	0.267	GAL	115	128		
306.1	0.441	GAL	305	224	avg. of Z, Z2(AEZO), HL and YMP	
313.0	0.461	GAL	744	359	avg. of Z, Z2(AEZO) and HL	
319.0	0.192	GAL	494	109		
320.0	0.342	GAL	856	145		
323.1	0.264	QSO	268	127		
327.1	0.4628	GAL	-195	181	YMP	
330.0	0.550	GAL	660	231	HL	
332.0	0.1515	GAL	306	101		
334.0	0.555	QSO	187	220	YE	
341.0	0.448	GAL	324	282	avg. of Z, Z2(AEZO) and HL	
345.0	0.594	QSO	773	297	YE	
346.0	0.161	GAL	641	104		
348.0	0.154	GAL	614	101		
349.0	0.205	GAL	206	112		
351.0	0.371	QSO	-82	146		
357.0	0.1664	GAL	370	103		
379.1	0.256	GAL	-136	126		
381.0	0.1605	GAL	138	103		
401.0	0.201	GAL	1131	112		
427.1	0.572	GAL	-166	289		
434.0	0.322	GAL	135	146		
435.0A	0.471	GAL	573-1273		YMP, Z	
436.0	0.2145	GAL	420	115		
455.0	0.5427	QSO	764	366	YE	
456.0	0.2330	GAL	-85	116		
458.0	0.290	GAL	101	129		
459.0	0.2199	N	33	116		
460.0	0.268	GAL	-110	128		

Note. —

- (1) We have no g frames for this field. There is a very bright star near the object.
- (2) We have no g frames for this field. The ID of this object is uncertain.
- (3) There is a very bright star near the object.
- (4) Although the error bars for the different B_{gg} values overlap, the B_{gg} values themselves differ by more than an Abell richness class (400 B_{gg} units).
- (5) The Z2(Z) and HL values agree with each other but are inconsistent with the value of YMP which is greater than these values by more than an Abell richness class.
- (6) The values of HL and YMP are not consistent with one another. However, these values differ by less than an Abell richness class and both are in agreement with the values of Z and Z2(AEZO). Thus, all values are used in the